Chem Soc Rev

REVIEW ARTICLE

View Article Online
View Journal | View Issue

# Fluorescent proteins for live-cell imaging with super-resolution

Cite this: *Chem. Soc. Rev.*, 2014, 43, 1088

Karin Nienhaus[a] and G. Ulrich Nienhaus*[abc]

Fluorescent proteins (FPs) from the GFP family have become indispensable as marker tools for imaging live cells, tissues and entire organisms. A wide variety of these proteins have been isolated from natural sources and engineered to optimize their properties as genetically encoded markers. Here we review recent developments in this field. A special focus is placed on photoactivatable FPs, for which the fluorescence emission can be controlled by light irradiation at specific wavelengths. They enable regional optical marking in pulse-chase experiments on live cells and tissues, and they are essential marker tools for live-cell optical imaging with super-resolution. Photoconvertible FPs, which can be activated irreversibly *via* a photo-induced chemical reaction that either turns on their emission or changes their emission wavelength, are excellent markers for localization-based super-resolution microscopy (*e.g.*, PALM). Patterned illumination microscopy (*e.g.*, RESOLFT), however, requires markers that can be reversibly photoactivated many times. Photoswitchable FPs can be toggled repeatedly between a fluorescent and a non-fluorescent state by means of a light-induced chromophore isomerization coupled to a protonation reaction. We discuss the mechanistic origins of the effect and illustrate how photoswitchable FPs are employed in RESOLFT imaging. For this purpose, special FP variants with low switching fatigue have been introduced in recent years. Despite nearly two decades of FP engineering by many laboratories, there is still room for further improvement of these important markers for live cell imaging.

Received 28th May 2013

DOI: 10.1039/c3cs60171d

www.rsc.org/csr



## 1. Introduction

Optical microscopy is one of the key biophysical methods in current life sciences research. Fluorescence microscopy, in particular, allows biological processes to be studied as they occur in space and time, both on the cellular and molecular levels. In conventional fluorescence microscopy, light emitted by fluorophores is collected by the objective lens and interferes in the image plane so as to form an image. Unfortunately, the (lateral) image resolution is limited to about half the wavelength of the light used for imaging due to diffraction, as stated by Abbe's famous law.[1] To achieve sub-diffraction resolution, or super-resolution, the emission from fluorophores that are closer in distance than $\sim$200 nm has to be detected sequentially rather than simultaneously, which is conveniently achieved *via* external control over the emission properties of the markers by light irradiation. To this end, one can actively define regions in the sample where the fluorescence is switched on by patterned illumination approaches such as stimulated emission depletion microscopy (STED), reversible saturable optical fluorescence transitions microscopy (RESOLFT), or saturated structured illumination (SSIM) microscopy.[2–6] Alternatively, one can observe individual fluorophores that are switched on stochastically and localize them with high precision as in localization microscopy (photoactivated localization microscopy (PALM), fluorescence photoactivation localization microscopy (FPALM), stochastical optical reconstruction microscopy (STORM)).[7–10] A third, most intriguing approach, super-resolution optical fluctuation imaging (SOFI), is based on the analysis of spatio-temporal correlations of intensity fluctuations observed in a time sequence of images, which come about because the photons are emitted by individual sources.[11] A refined version, balanced SOFI (bSOFI), has been introduced lately.[12] The basic principles of the super-resolution imaging techniques will be discussed briefly below; details can be found in recent reviews.[13–18]

As the intrinsic fluorescence of biological molecules is weak and non-specific and, therefore, of limited use for imaging applications, a wide array of fluorescent labels and activatable probes have been developed. Among the markers presently available, *i.e.*, synthetic dyes,[19] nanocrystals,[20–24] and fluorescent

[a] *Institute of Applied Physics and Center for Functional Nanostructures (CFN), Karlsruhe Institute of Technology (KIT), Wolfgang-Gaede-Straße 1, 76131 Karlsruhe, Germany*
[b] *Institute of Toxicology and Genetics, Karlsruhe Institute of Technology (KIT), 76344 Eggenstein-Leopoldshafen, Germany*
[c] *Department of Physics, University of Illinois at Urbana-Champaign, 1110 West Green Street, Urbana, IL 61801, USA. E-mail: uli@illinois.edu; Tel: +49 (0)721 608 43401*

proteins (FPs),[25–28] FPs have the key advantage that they are genetically encodable, so they can be produced by the cells and organisms themselves. Consequently, there is no need for additional labeling and/or other chemical procedures in studies of live cells and organisms.

The first FP labels employed in cellular biology were phycobiliproteins, *i.e.*, photosynthetic antenna pigments extracted from cyanobacteria.[29] Their applicability as intracellular fluorescent labels is restricted, however, by their large size and the need to supply a tetrapyrrole cofactor. Monomeric, infrared-fluorescent variants of a bacteriophytochrome from *Deinococcus radiodurans* with a biliverdin chromophore have been reported and may find broader applicability in the future.[30] Recently, the first FP in a vertebrate, UnaG, was identified, which contains a noncovalently bound bilirubin chromophore.[31]

The green fluorescent protein, GFP, and the entire GFP family of proteins, however, do not require any additional enzyme or cofactor to form functional fluorescence markers. GFP was discovered in 1962 by Osamu Shimomura in tissue extracts of the jellyfish *Aequorea victoria*.[32] Only in 1994, when the GFP gene[33] was expressed recombinantly in *Escherichia coli* and *Caenorhabditis elegans* by Martin Chalfie and co-workers,[34] it was realized that GFP forms spontaneously and thus can be employed as a genetically encoded fluorescence marker. Subsequently, advanced variants of *A. victoria* GFP (avGFP) were developed by Tsien, with emission peaks ranging from blue (BFP) to yellow (YFP).[35] The award of the Nobel Prize in Chemistry in 2008 to Shimomura, Chalfie, and Tsien testifies to the enormous resonance of GFP marker technology in the research community.[36–38] Homologs of GFP were discovered in anthozoa and other animals.[39–44] Some of these variants had attractive new properties for marker applications, such as emission in the red spectral region[45,46] and light-activatable fluorescence changes.[47–49] The further development and application of advanced FPs have been ongoing ever since. Presently, FPs play a key role in the life sciences, *e.g.*, in cellular imaging,[27] in clinical research and also in the pharmaceutical industry.[50,51] As yet, more than 1000 FP variants have been reported; a small but representative selection is compiled in Tables 1–3. From these tables, FPs can be selected on the basis of their photophysical parameters. However, whether or not a particular FP will allow excellent experimental data to be obtained still depends on the details of the experimental design.[52]

## 2. General characteristics of the GFP family of proteins

### 2.1 Structural properties

The polypeptide chain of GFP-like proteins consists of ~230 amino acids. It folds into a rigid, 11-stranded β-can (Fig. 1a),[53,54] capped at either end by short helical sections and loops. The fluorescent chromophore, which interrupts a helix running along the central axis, resides close to the geometric center of the protein. Surrounding residues and structural water molecules anchor the chromophore and, ideally, should hold it in a planar conformation, which is essential for a high fluorescence quantum yield (QY). However, only few crystal structures show perfectly planar chromophores. In general, the protein matrix forces the aromatic ring of Tyr66 to slightly twist around the Cα═Cβ double bond of the ethylenic bridge, which is supposed to prevent more prominent deformations.[55] The GFP chromophore, 4-(*p*-hydroxybenzylidene)-5-imidazolinone (*p*-HBI), forms autocatalytically from a tripeptide (Ser65-Tyr66-Gly67 in avGFP, Fig. 1b). Chromophore maturation requires no further ingredients except for molecular oxygen ($O_2$). The first amino acid in the chromophoric triad may vary among natural FPs, the Tyr and Gly residues, however, are strictly conserved. The only known exceptions, GFP-like proteins from the lancelet *Branchiostoma floridae*, containing a Gly-Tyr-Ala tripeptide, are essentially nonfluorescent.[56,57] Additional chemical modifications of the *p*-HBI chromophore have been found in many FPs that can further extend the delocalized π-electron system. For example, in red FPs (RFPs) such as DsRed from *Discosoma* sp.[42] or eqFP611,[58] the bond between the amide nitrogen

**Karin Nienhaus**

*Karin Nienhaus studied chemistry at the University of Münster, Germany. In 2003, she received her PhD degree in Chemistry at the University of Ulm, Germany. From 2000 to 2009, she worked as a Research Assistant at the Institute of Biophysics in Ulm. Since 2009, she has been working as a Research Associate at the Institute of Applied Physics, Karlsruhe Institute of Technology (KIT), Germany. Her work focuses on investigating the molecular details of enzyme–substrate–ligand interactions and photoactivated processes in fluorescent proteins using various steady-state and time-resolved spectroscopic approaches.*

**G. Ulrich Nienhaus**

*Gerd Ulrich Nienhaus is Chair Professor and Head of the Institute of Applied Physics, Karlsruhe Institute of Technology (KIT), Germany. He studied Physics and received his PhD degree in Physical Chemistry from the University of Münster, Germany, in 1988. In 1990, he joined the Department of Physics of the University of Illinois at Urbana-Champaign, USA. In 1996, he accepted an offer to become Chair Professor and Head of the Institute of Biophysics at the University of Ulm, Germany. In 2009, he joined the KIT. His research is focused on molecular and cellular biophysics using a broad array of biophotonics techniques including spectroscopy and advanced fluorescence microscopy.*

Table 1 Optical properties of monomeric, not photoactivatable FPs

| FP | Ex. max. (nm) | Em. max. (nm) | p*K* | QY | $\varepsilon$ ($M^{-1}$ $cm^{-1}$) | Ref. |
|---|---|---|---|---|---|---|
| Sirius | 355 | 424 | <3.0 | 0.24 | 15 000 | 207 |
| Azurite | 383 | 447 | 5.0 | 0.55 | 26 000 | 208 |
| EBFP2 | 383 | 448 | 4.5 | 0.56 | 32 000 | 209 |
| TagBFP | 402 | 457 | 2.7 | 0.63 | 52 000 | 210 |
| mTurquoise2 | 434 | 474 | 4.5 | 0.93 | 30 000 | 211 |
| Cerulean | 433 | 475 | 4.7 | 0.57 | 36 000 | 212 |
| ECFP | 434 | 477 | 4.7 | 0.4 | 32 500 | 213 |
| TagCFP | 458 | 480 | 4.7 | 0.57 | 37 000 | Evrogen |
| mTFP1 | 462 | 492 | 4.3 | 0.85 | 64 000 | 214 |
| mUkG1 | 483 | 499 | 5.2 | 0.72 | 60 000 | 215 |
| AcGFP1 | 475 | 505 | | 0.55 | 50 000 | 110 |
| mAG1 | 492 | 505 | 5.8 | 0.74 | 55 000 | 216 |
| TagGFP2 | 483 | 506 | 5.0 | 0.61 | 56 500 | 210 |
| EmGFP | 487 | 509 | 6.0 | 0.68 | 57 500 | 217 |
| EGFP | 489 | 509 | 5.9 | 0.6 | 55 000 | 157 |
| mWasabi | 493 | 509 | 6.5 | 0.8 | 70 000 | 218 |
| T-Sapphire | 399 | 511 | 4.9 | 0.6 | 44 000 | 219 |
| Clover | 505 | 515 | 6.2 | 0.76 | 111 000 | 170 |
| mNeonGreen | 506 | 517 | 5.7 | 0.80 | 116 000 | 220 |
| TagYFP | 508 | 524 | 5.5 | 0.62 | 64 000 | Evrogen |
| mAmetrine | 406 | 526 | 6.0 | 0.58 | 45 000 | 167 |
| EYFP | 514 | 527 | 6.5 | 0.61 | 84 000 | 221 |
| Topaz | 514 | 527 | | 0.6 | 94 500 | 217 |
| SYFP2 | 515 | 527 | 6.0 | 0.68 | 101 000 | 169 |
| Venus | 515 | 528 | 6.0 | 0.57 | 92 200 | 222 |
| Citrine | 516 | 529 | 5.7 | 0.76 | 77 000 | 223 |
| mKO | 548 | 559 | 5.0 | 0.6 | 51 600 | 168 |
| mOrange | 548 | 562 | 6.5 | 0.69 | 71 000 | 43 |
| mOrange2 | 549 | 565 | 6.5 | 0.6 | 58 000 | 224 |
| mKO2 | 551 | 565 | 5.5 | 0.57 | 63 800 | 225 |
| TagRFP | 555 | 584 | <4.0 | 0.48 | 100 000 | 106 |
| TagRFP-T | 555 | 584 | 4.6 | 0.41 | 81 000 | 224 |
| mStrawberry | 574 | 596 | <4.5 | 0.29 | 90 000 | 43 |
| mRuby | 558 | 605 | 4.4 | 0.35 | 112 000 | 71 |
| mRuby2 | 559 | 600 | 5.3 | 0.38 | 113 000 | 170 |
| mCherry | 587 | 610 | <4.5 | 0.22 | 72 000 | 43 |
| mKeima | 440 | 620 | 6.5 | 0.24 | 14 400 | 226 |
| mRaspberry | 598 | 625 | | 0.15 | 86 000 | 227 |
| mKate2 | 588 | 633 | 5.4 | 0.4 | 62 500 | 178 |
| mPlum | 590 | 649 | <4.5 | 0.1 | 41 000 | 227 |
| mNeptune | 600 | 650 | 5.4 | 0.2 | 67 000 | 175 |
| TagRFP657 | 611 | 657 | 5.0 | 0.1 | 34 000 | 228 |
| TagRFP675 | 598 | 675 | 5.7 | 0.08 | 46 000 | 229 |
| LSSmOrange | 437 | 572 | 5.7 | 0.45 | 52 000 | 86 |
| LSSmKate1 | 463 | 624 | 3.2 | 0.08 | 31 200 | 87 |
| LSSmKate2 | 460 | 605 | 2.7 | 0.17 | 26 000 | 87 |
| Low-FT | 402/583 | 465/604 | 2.6/4.6 | 0.35/0.05 | 33 400/84 200 | 230 |
| Medium-FT | 401/579 | 464/600 | 2.7/4.7 | 0.41/0.08 | 44 800/73 100 | 230 |
| Fast-FT | 403/583 | 466/606 | 2.8/4.1 | 0.30/0.09 | 49 700/75 300 | 230 |
| mK-GO | 500/548 | 509/561 | 6.0/4.8 | — | 35 900/42 000 | 231 |

and the Cα atom of the first residue of the chromophore-forming triad is oxidized to an acylimine group coplanar with the *p*-HBI chromophore. Other chromophore modifications have been revealed in, *e.g.*, zFP538,[59] mOrange,[60] and AsRed.[61]

GFP-like proteins are typically oligomeric in nature. Some FPs form strongly associated dimers, *e.g.*, GFP from the sea pansy *Renilla*[62] or phiYFP from the jellyfish *Phialidium*.[63] Anthozoan FPs are often found as tightly associated tetramers, with the four protomers A–D arranged as dimers of dimers (Fig. 1a).[42,58]

### 2.2 Optical properties

The isolated *p*-HBI chromophore can adopt the *cis* or the *trans* configuration, as shown in Fig. 2. In most natural FPs, the folded polypeptide chain enshrouds a *cis* chromophore. In either isomeric state, the hydroxyphenyl moiety of the chromophore can, in principle, be protonated (neutral) or deprotonated (anionic). The two protonation species can easily be distinguished by their characteristic absorption spectra (Fig. 2). The spectra of the neutral (A) chromophore are markedly blue-shifted from those of the anionic (B) form. The absorption bands of the *cis* and *trans* chromophores overlap significantly; if *cis* and *trans* species in the same protonation state coexist in a sample, they will both be excited by the same wavelength.

Typically, but not always,[64–66] the equilibrium between the neutral and anionic forms can be controlled by the solvent pH, indicating that protons can easily migrate to the protonation

 

Table 2 Optical properties of monomeric photoconvertible FPs

| | Inactivated | | | Activated | | | | | | |
|---|---|---|---|---|---|---|---|---|---|---|
| Name | Ex. max. (nm) | Em. max (nm) | Activat. light (nm) | Exc. max (nm) | Em. max (nm) | On/off ratio | p$K$ | $\varepsilon$ ($M^{-1}$ $cm^{-1}$) | QY | Ref. |
| PAGFP | | | 405 | 504 | 517 | 70 | | | | 97 |
| PATagRFP | | | 405 | 562 | 595 | 540 | 0.38 | 66 000 | 0.38 | 107 |
| PAmCherry1 | | | 405 | 564 | 595 | 4000 | 0.46 | 18 000 | 0.46 | 73 |
| PAmRFP-1 | | | 405 | 578 | 605 | 70 | 0.08 | 10 000 | 0.08 | 104 |
| PAmKate | | | 405 | 586 | 628 | 100 | 0.18 | 25 000 | 0.18 | 108 |
| PS-CFP (C)[a] | 402 | 468 | 405 | | | 300 | | 34 000 | 0.16 | 111 |
| PS-CFP (G)[a] | | | | 490 | 511 | 1500 | | 27 000 | 0.19 | 111 |
| PS-CFP2 (C) | 400 | | 405 | | | | 4.6 | 43 000 | 0.2 | 111 |
| PS-CFP2 (G) | | 468 | | 490 | 511 | | 6.1 | 47 000 | 0.23 | 111 |
| Dendra2 (G) | 490 | 507 | 405, 488 | | | | 7.1 | 45 000 | 0.50 | 115 |
| Dendra2 (R)[a] | | | | 553 | 573 | 300 | 7.5 | 35 000 | 0.55 | 115 |
| mKikGR (G) | 505 | 515 | | | | | — | 49 000 | 0.69 | 129 |
| mKikGR (R) | | | | 580 | 591 | 400 | — | 28 000 | 0.63 | 129 |
| mEosFP (G) | 506 | 516 | 405 | | | | 5.8 | 72 000 | 0.70 | 113 |
| mEosFP (R) | | | | 571 | 581 | | 5.8 | 41 000 | 0.62 | 113 |
| mEos3.1 (G) | 505 | 513 | 405 | | | | | 88 400 | 0.83 | 127 |
| mEos3.1 (R) | | | | 570 | 580 | | | 33 500 | 0.62 | 127 |
| mEos3.2 (G) | 507 | 516 | 405 | | | | | 63 400 | 0.84 | 127 |
| mEos3.2 (R) | | | | 572 | 580 | | | 32 200 | 0.55 | 127 |
| mEos2 (G) | 506 | 519 | 405 | | | | 5.6 | 56 000 | 0.84 | 125 |
| mEos2 (R) | | | | 573 | 584 | | 6.4 | 46 000 | 0.66 | 125 |
| mIrisFP (G) | 486 | 516 | 405 | | | | 5.4 | 47 000 | 0.54 | 153 |
| mIrisFP (R) | | | | 546 | 578 | | 7.6 | 33 000 | 0.59 | 153 |
| PSmOrange | 548 | 565 | 488 | | | | | 113 300 | 0.51 | 130 |
| PSmOrange (R) | | | | 636 | 662 | 560 | | 32 700 | 0.28 | 130 |
| mClavGR2 (G) | 488 | 504 | 405 | | | | | 19 000 | 0.77 | 118 |
| mClavGR2 (R) | | | | 566 | 583 | | | 32 000 | 0.35 | 118 |
| mMaple (G) | 489 | 505 | 405 | | | | 8.2 | 15 000 | 0.74 | 119 |
| mMaple (R) | | | | 566 | 583 | | 7.3 | 30 000 | 0.56 | 119 |
| NijiFP (G) | 469 | 507 | 405 | | | | 7.0 | 41 100 | 0.64 | 128 |
| NijiFP (R) | | | | 526 | 569 | | 7.3 | 42 000 | 0.65 | 128 |
| Phamret (C) | 458 | 475 | 405 | | | | | 32 500 | 0.40 | 101 |
| Phamret (G) | | | | 458 | 517 | | | 17 400 | 0.79 | 101 |

[a] (C): cyan; (G): green; (R): red.

site inside the β-can. The proton affinity of the hydroxyphenyl group, characterized by an equilibrium coefficient, or p$K$ (Tables 1–3), depends on the local environment and can be varied markedly by amino acid exchanges. Green and yellow FPs usually have $5.0 < pK < 7.0$,[67] whereas blue and far-red variants often show $pK < 4$.[67] Biological processes may involve substantial changes in pH, *e.g.*, acidification in endocytic vesicles. In such cases, the pH dependence of the protonation equilibrium and the resulting changes in the fluorescence properties need to be taken into account. However, one can also exploit this effect by using FPs as nanoscale probes of local pH within living cells.[68,69]

Most often, the anionic *cis* chromophore is the brightly fluorescent species; only a few FPs are known to feature a fluorescent anionic *trans* chromophore.[58,70–75] In some FPs including avGFP or asFP499, absorption of light by the neutral chromophore results in emission by an anionic species because of excited state proton transfer (ESPT), during which the proton is ejected from the hydroxyphenyl moiety so as to form an anionic species.[76–81] There are also several examples of direct emission from the neutral chromophore, *e.g.*, in avGFP variants,[82,83] dual emission pH sensors[69,84] and anion-bound EYFP.[85] ESPT is also responsible for the large Stokes shifts of LSSmOrange,[86] LSSmKate1 and LSSmKate2.[87] By introducing additional carboxyl groups at suitable positions to provide an ESPT pathway, large Stokes shifts were achieved in several RFPs including mNeptune, mCherry, mStrawberry, mOrange, and mKO.[88]

Table 3 Optical properties of monomeric photoswitchable FPs

| FP | Ex. max. (nm) | Em. max. (nm) | On/off contrast | Activating light on–off (nm) | p*K* | $\varepsilon$ ($M^{-1}$ $cm^{-1}$) | QY | Ref. |
|---|---|---|---|---|---|---|---|---|
| mTFP0.7 | 453 | 488 | | 405–450 | 4.0 | 60 000 | 0.5 | 133 |
| rsEGFP2 | 478 | 503 | | 405–488 | | 61 000 | 0.3 | 158 |
| bsDronpa | 460 | 504 | 17 | 405–488 | | 45 000 | 0.5 | 146 |
| NijiFP (G)[a] | 469 | 507 | | 405–488 | 7.0 | 41 100 | 0.64 | 128 |
| Mut2Q | 496 | 507 | | 405–488 | 6.0 | 54 000 | 0.28 | 155 |
| rsEGFP | 493 | 510 | | 405–488 | 6.5 | 47 000 | 0.36 | 156 |
| mGeos-S | 501 | 512 | | 405–488 | 5.0–5.5 | 64 602 | 0.76 | 152 |
| mGeos-E | 501 | 513 | | 405–488 | 6.0–6.5 | 69 630 | 0.75 | 152 |
| mGeos-L | 501 | 513 | | 405–488 | 5.0–5.5 | 53 448 | 0.72 | 152 |
| mGeos-M | 503 | 514 | | 405–488 | 4.5–5.0 | 51 609 | 0.85 | 152 |
| Dronpa-2 | 489 | 515 | | 405–488 | | 56 000 | 0.28 | 232 |
| Dronpa-3 | 489 | 515 | | 405–488 | | 58 000 | 0.33 | 232 |
| mGeos-F | 504 | 515 | | 405–488 | 5.0 | 53 135 | 0.85 | 152 |
| mIrisFP (G) | 486 | 516 | | 405–488 | 5.7 | 47 000 | 0.54 | 153 |
| mIrisGFP | 488 | 516 | | 405–488 | 5.3, 6.0 | 47 000 | 0.63 | 135 |
| mGeos-C | 505 | 516 | | 405–488 | 6.0 | 76 967 | 0.81 | 152 |
| Dronpa | 503 | 517 | Good | 405–488 | | 94 100 | 0.67 | 143 |
| rsFastLime | 496 | 518 | 67 | 405–488 | | 39 094 | 0.77 | 146 |
| Padron | 503 | 522 | 143 | 488–405 | | 43 000 | 0.64 | 149 |
| EYQ1 | 510 | 524 | | 405–488 | 6.9 | 73 000 | 0.72 | 155 |
| Dreiklang | 511 | 529 | | 365–405 | 7.2 | 83 000 | 0.41 | 131 |
| NijiFP (R)[a] | 526 | 569 | | 440–561 | 7.3 | 42 000 | 0.65 | 128 |
| MIrisFP (R) | 546 | 578 | | 440–561 | 7.0 | 33 000 | 0.59 | 153 |
| rsTagRFP | 567 | 585 | | 450–570 | 6.6 | 36 800 | 0.11 | 233 |
| rsCherryRev | 572 | 608 | 20 | 450–550 | 5.5 | 84 000 | 0.005 | 140 |
| rsCherry | 572 | 610 | 6.7 | 550–450 | 6.0 | 80 000 | 0.02 | 140 |

[a] (G): green; (R): red.

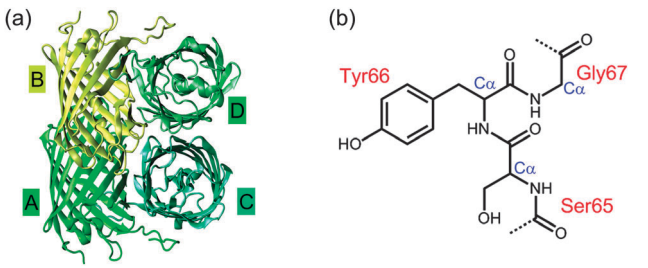


Fig. 1 Structural properties of GFP-like proteins. (a) Tetrameric arrangement of the four protomers. (b) Chromophore-forming tripeptide of avGFP.

A good fluorescent marker must have a high tendency to capture photons, *i.e.*, a large absorption cross section, combined with a high QY of fluorescence emission (Tables 1–3). Consequently, the molecular brightness is defined as the product of the peak extinction coefficient and the QY. Sometimes, the relative molecular brightness, *i.e.*, the molecular brightness with respect to that of EGFP, is quoted for comparison of different FPs.[67,89] FPs can also be excited by a two-photon process, which can be useful for 4Pi microscopy[90] or imaging of thick specimens.[90]

The fluorophores of FPs, like many synthetic fluorophores, have a tendency to incessantly switch between a fluorescent and a nonemissive state under excitation.[90–93] This intermittent behavior is completely obscured in bulk experiments but becomes very obvious in studies at the single-molecule level. It can be a nuisance for some applications, *e.g.*, single-particle tracking, but is a necessary ingredient for others including super-resolution imaging.[94,95]

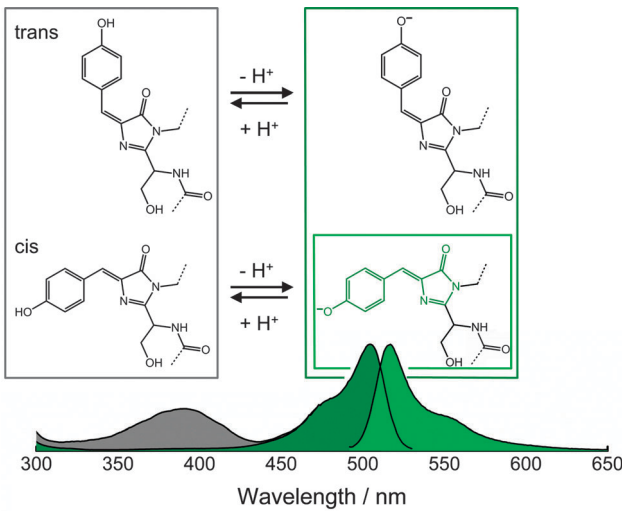


Fig. 2 Relevant isomeric and protonation states of the GFP chromophore. The protonated *trans* and *cis* isomers (gray box) display characteristic A absorption bands at ~390 nm (area shaded in gray). The anionic species (dark green box) give rise to B absorption bands at ~500 nm (shaded in dark green). Typically, only the anionic *cis* chromophore (bright green box) is brightly fluorescent (emission band shaded in bright green) in the temperature range used for live-cell imaging.

## 3. Photoactivatable FPs

In recent years, 'photoactivatable' or 'optical highlighter' FPs (PA-FPs) have emerged as especially powerful marker tools for live-cell imaging applications.[47,96] Their fluorescence properties can be modified by light irradiation at specific wavelengths.

 

Irreversible photoactivation (photoconversion) involves a permanent photochemical modification of the FP. As a consequence, a non-fluorescent (dark) state may get permanently activated to a fluorescent (bright) state, or a bright state may be turned into another bright state with a different emission wavelength. A list of representative photoconvertible FPs is given in Table 2. Reversible photoactivation (photoswitching) typically arises from chromophore isomerization between two configurations, only one of which emits fluorescence with high yield. Table 3 contains a selection of photoswitchable FPs.

### 3.1 Irreversible off–on photoactivation

The first FP that was advertised as being photoactivatable, PA-GFP,[97] emits fluorescence only after irradiation with intense violet (~400 nm) light (Table 2). X-ray structure analysis revealed that photoconversion involves a light-induced decarboxylation of Glu222 that shifts the chromophore equilibrium from the dark, neutral *cis* to the brightly fluorescent, anionic *cis* form (Fig. 3a),[98] thereby causing a ~100-fold enhancement of the fluorescence. PA-GFP has been successfully employed in a wide variety of applications.[7,99–102]

Phamret is a photoactivatable, engineered protein construct that consists of two FP units, PA-GFP and an enhanced cyan FP (ECFP) variant, connected *via* a two-amino acid linker in a so-called tandem dimer arrangement.[101] Upon excitation with 458-nm light, the ECFP subunit emits cyan fluorescence at 475 nm (Table 2). After photoactivation of the PA-GFP subunit at 400 nm, Phamret exhibits green fluorescence peaking at 517 nm due to FRET between the two subunits. Only a single excitation wavelength is required; the dimeric nature of Phamret, however, may cause problems in some applications, *e.g.*, as a fusion marker.

Photoactivatable monomeric RFPs (PAmRFPs) have been derived from the monomeric variant of DsRed, mRFP1.[42,103] They can be photoconverted irreversibly from a dark to a red-emitting state by illumination with violet light (Table 2). The brightest variant, PAmRFP1, shows a ~70-fold increase in red fluorescence upon photoactivation,[104] but lacks the high photon yields required for single molecule-based imaging applications such as PALM. The PAmCherry proteins,[73] derived from mCherry, are advanced variants of PAmRFP1 that are essentially non-fluorescent prior to photoactivation (Table 2). Illumination with violet light leads to a 3000–5000-fold fluorescence enhancement and renders them permanently red fluorescent.[73] Initially, PAmCherry1 exhibits a non-coplanar anionic DsRed-like chromophore in the *trans* configuration. Upon activation, $CO_2$ is released from the Glu215 side chain. The ensuing oxidation of the Tyr67 Cα–Cβ bond extends the conjugated π-electron system and forms the red-fluorescent *trans* chromophore (Fig. 3b).[105] The monomeric variant of TagRFP,[106] PATagRFP,[107] is also initially dark and turns red fluorescent after irradiation with violet light. PAmKate[108] is a derivative of mKate[109] with a far red-shifted emission ($\lambda_{em}$ = 628 nm) after photoactivation with 405 nm-light.

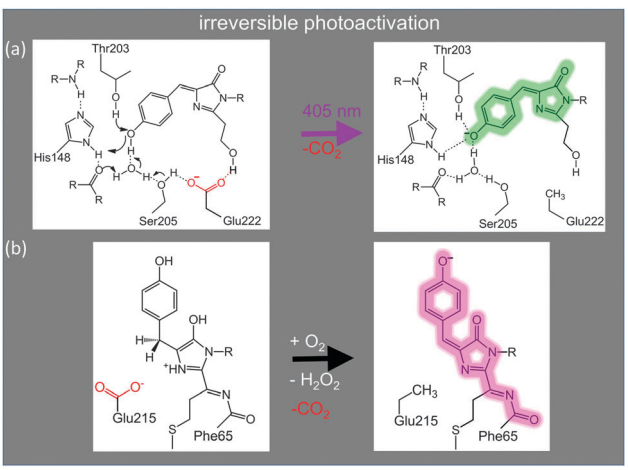


Fig. 3 Irreversible photoactivation from a dark to a bright state for (a) PA-GFP and (b) PAmCherry.

### 3.2 Irreversible photoactivation by shifting the emission wavelength

The cyan PS-CFP, which was engineered from the non-fluorescent FP acGFPL,[110] can be photoactivated with ~400 nm light. A 300-fold increase in green and a 5-fold decrease in cyan fluorescence together yield an overall 1500-fold increase in the green-to-cyan fluorescence ratio (Table 2).[111] As for PA-GFP, light-induced decarboxylation of Glu215 and the concomitant deprotonation of the chromophore hydroxyphenyl are responsible for this effect. An enhanced version, PS-CFP2, has also been reported, which is twice as bright as PS-CFP and has a contrast ratio of 2000.[112]

Another class of photoconvertible FPs comprises Kaede,[48] EosFP,[113,114] Dendra2,[115,116] KikGr,[117] mClavGR2,[118] and mMaple (Table 2).[119] In these FPs, which all have a histidine at the first position of the chromophore-forming tri-peptide, irradiation into the absorption band of the neutral green chromophore (~400 nm, Fig. 2) causes an irreversible shift of the emission from green to red. Photoconversion to the red-emitting form (~580 nm) is accompanied by cleavage of the peptide backbone between the Nα and Cα atoms of the histidine (Fig. 4, dark gray box). Concomitantly, a double bond forms between its Cα and Cβ atoms, so that the conjugated π-electron system of the chromophore is extended toward the histidine imidazole ring.[120–123] Both the green and red forms of EosFP can efficiently be excited *via* two-photon absorption; photoconversion also occurs by absorption of two 800 nm photons.[90] Improved monomeric variants of EosFP,[124–127] Dendra[128] and KikGr[129] (Table 2) feature very high contrast ratios between the activated and deactivated states at the probe wavelengths in the red region of the spectrum.

Monomeric PSmOrange is initially orange-fluorescent and becomes far-red fluorescent after irradiation with blue-green light (Table 2).[130] Currently, PSmOrange exhibits the longest excitation wavelength of all GFP-like FPs in its photoactivated form ($\lambda_{exc}$ = 636 nm) and, therefore, can conveniently be excited with common red diode lasers.

### 3.3 Reversible photoactivation

Reversibly photoactivatable, or photoswitchable FPs (PS-FPs, Table 3) can be toggled between a dark off and a bright on state by light irradiation. Apart from a notable exception (Dreiklang),[131]

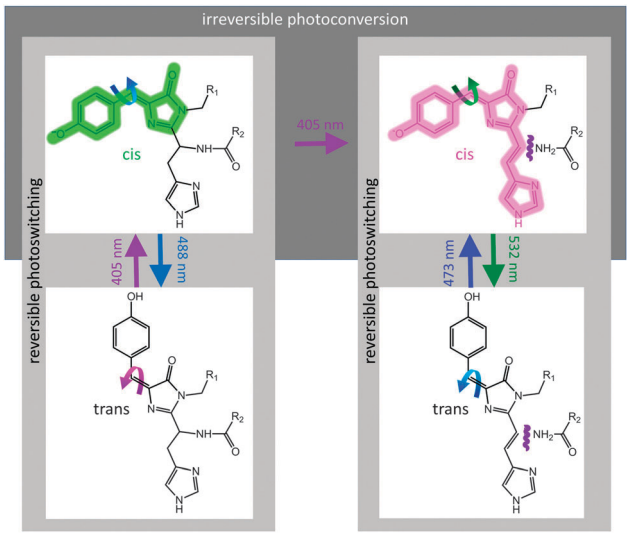


Fig. 4 Reversible photoswitching (light gray frames) of the green and red chromophores and irreversible photoconversion (marked in dark gray) from green to red in mIrisFP.

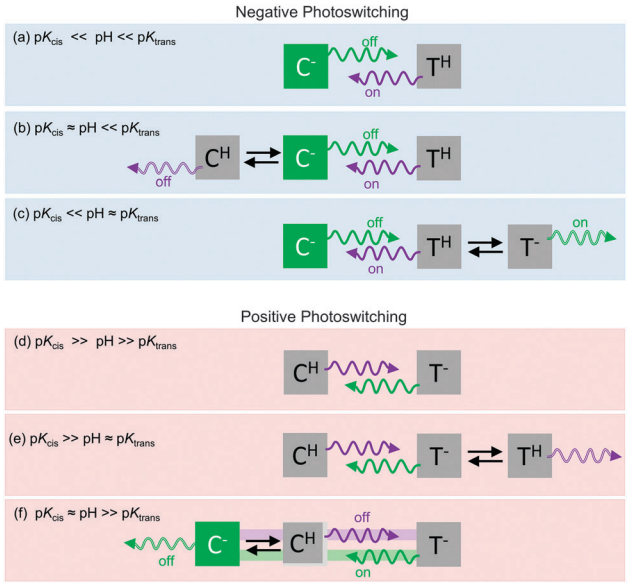


Fig. 5 Reversible photoactivation, (a–c) negative photoswitching, (d–f) positive photoswitching. *cis* and *trans* chromophores are denoted by C and T, respectively, with superscripts 'H' for neutral and '–' for anionic. Solid violet and green arrows represent the photoactivation light. Black arrows denote thermal equilibrium as given by the p*K*. Arrows with open shafts indicate secondary effects of the activation light.

all PS-FPs utilize a photoswitching mechanism that involves a change of the chromophore's isomerization and protonation states (Fig. 4, light gray boxes), which is accompanied by conformational rearrangements of amino acids in the chromophore environment.[132–135] Most often, the *cis* configuration is the thermodynamically stable state in PS-FPs; its anionic form constitutes the fluorescent form.[132,136] For a few photoswitchers, the non-fluorescent *trans* state is the stable species, and light irradiation induces a *trans–cis* isomerization to the fluorescent *cis* state.[137,138] In the dark, all PS-FPs relax spontaneously to their stable isomeric states on time scales ranging from minutes to hours. Relaxation can also be driven by light irradiation of a suitable wavelength, which accelerates the process markedly.

In general, a PS-FP may assume four conformations, associated with a neutral or anionic *cis* ($C^H$, $C^-$) or a neutral or anionic *trans* ($T^H$, $T^-$) chromophore. As light-activated chromophore isomerization is typically accompanied by a change in the protonation state, the photoswitching properties depend crucially on the proton affinities of the hydroxyphenyl groups of the two isomers in the ground and excited states, quantified by $pK_{cis}$ and $pK_{trans}$, and on details of the energy surfaces connecting the different states.[139] Of course, proton-accepting and -donating groups have to be available for proton exchange to occur and, in addition, isomerization has to be sterically feasible.

In the following, we briefly discuss the chromophore transitions caused by irradiation of a PS-FP. For simplicity, we assume that $C^-$ is the only chromophore species emitting fluorescence photons in the green and that the sample pH is close to neutral, which is predominantly the case in live cell imaging. If $pK_{cis} < pH_{sample} < pK_{trans}$, only two fluorophore species, $C^-$ and $T^H$, will be populated appreciably in equilibrium. Green light excites $C^-$ (Fig. 5a) and, usually with a low probability, causes it to switch to the non-fluorescent $T^H$ form. Thus, a burst of fluorescence photons occurs which ceases upon photoisomerization. Blue light induces the reverse transition and, therefore, restores the $C^-$ species; the FP is switched back on. This scenario is characteristic of so-called negative photoswitchers, for which excitation of the fluorescent species also induces off switching.[140] If $pK_{cis} \approx pH_{sample} < pK_{trans}$, the neutral $C^H$ state becomes appreciably populated (Fig. 5b). Again, green light excites $C^-$ and, with a low quantum yield, induces a transition to the dark $T^H$ form. Blue light, however, causes excitation of both $T^H$ and $C^H$ *via* their A bands, so that *trans–cis* and *cis–trans* isomerization reactions are activated. The overall result is a reduced fraction of the $C^-$ species; on switching is incomplete.[135] Similarly, for $pK_{cis} < pH_{sample} \approx pK_{trans}$, $T^-$ appears as a third state and gives rise to a more complicated behavior (Fig. 5c). The negative switching mode, however, is always maintained.

If the p*K*s are arranged in reverse order, and $pK_{cis} > pH_{sample} > pK_{trans}$, the non-fluorescent $C^H$ and $T^-$ species are essentially the only populated states. Photoisomerization between these species can be induced by light, but no fluorescence occurs because both $C^H$ and $T^-$ are non-emissive (Fig. 5d). If $pK_{cis} > pH \approx pK_{trans}$, $T^H$ is noticeably present, but there is again no change in fluorescence upon light-activated isomerization (Fig. 5e). If, however, $pK_{cis} \approx pH > pK_{trans}$ (Fig. 5f), excitation of $T^-$ with green light causes photoisomerization and thus enhances the $C^H$ population. Subsequently, $C^H$ population transforms into $C^-$ species so as to restore the protonation equilibrium. The net result of irradiating into the B band of $T^-$ is that the fraction of the fluorescent species, $C^-$, is enhanced. This scenario is characteristic of so-called positive photoswitchers, for which excitation within the spectral region of the B absorption band enhances the emission.[140] Note that it is not excitation of the

 

fluorescent species $C^-$, but rather the dark $T^-$ that causes an enhancement of $C^-$. Typically, the B band spectrum of $T^-$ is only slightly blue-shifted from the one of $C^-$ so that they both overlap strongly. The $C^-$ species will undergo *cis–trans* isomerization upon activation by green light, thereby reducing the fluorescence again. The net effect of irradiation into the B band depends on the relative populations of the species present and the associated photoisomerization QYs. The off transition is achieved by blue light excitation of $C^H$, which photoisomerizes to non-fluorescent $T^-$. Subsequently, the protonation equilibrium between $C^H$ and $C^-$ re-adjusts, which causes a reduction of the fluorescent $C^-$ species. In positive photoswitchers, both on and off transitions involve an adjustment of the protonation equilibrium between $C^H$ and $C^-$ in addition to photoinduced isomerization.

Dronpa, originally cloned from the stony coral *Echinophyllia* sp., is a well-studied negative photoswitcher.[49,132,141,142] It has been reported that bulk samples of Dronpa can undergo ~100 times on–off cycling with only 25% of fluorescence reduction.[143] Dronpa has served as a marker protein for high-resolution microscopy such as PALM[144] and RESOLFT.[145] rsFastLime, a variant of Dronpa with accelerated switching kinetics,[146] has been applied in PALMIRA imaging.[147,148] bsDronpa, a random mutant of rsFastLime, has spectral properties significantly different from its parental protein. Its excitation band is blue-shifted by ~40 nm ($\lambda_{exc}$ = 460 nm, Table 3). Notably, bsDronpa can still be excited with 400 nm light and has been employed in dual-color super-resolution microscopy using Dronpa as a second label.[149] Padron is yet another variant of rsFastLime.[149] This positive photoswitcher is practically non-fluorescent in thermal equilibrium (Table 3).[138,150] The dynamic range upon photoswitching is high, 150 : 1, and promises high contrast ratios in live-cell imaging applications. Codon-optimized variants of Dronpa and its derivatives have also been used for imaging transgenic *Arabidopsis thaliana* plants.[151] Monomeric teal FP, mTFP0.7, shows illumination-dependent spectral changes similar to those of Dronpa.[133]

Recently, a series of PS-FPs based on mEos2[125] have been presented.[152] In these variants, the histidine at the first position in the chromophoric triad was replaced so as to eliminate green-to-red photoconversion. The same effect was achieved by exchanging Phe173 in mEosFP*thermo*[126] by Ser.[128,153] The resulting variant, called mIrisGFP, has recently been employed to study reversible photoswitching in great detail.[135] In combination with EosFP*thermo*, mIrisGFP has been utilized in dual-color PALM experiments to investigate intermediate filament and aggregate formation by using fusion constructs with desmin mutants.[154]

Even avGFP from the jellyfish can be turned into a photoswitcher; examples are Mut2Q and EYQ1.[155] rsEGFP,[156] derived from EGFP,[157] shows very fast switching kinetics and was reported to endure more than 1000 photoswitching cycles. Because of its enormous switching stamina, it has enabled all-optical writing of features with subdiffraction size and spacings using the RESOLFT approach.[156] An advanced variant, rsEGFP2,[158] survives even more switching cycles.

Two variants of mCherry with opposite switching modes, rsCherry and rsCherryRev, were the first monomeric PS-FPs emitting in the red spectral range.[140] rsTagRFP, a photoswitchable version of TagRFP, offers an alternative to the negative photoswitcher rsCherryRev.[159] It was successfully employed in photochromic FRET experiments, where the fluorescence intensity of the donor was modulated by light-induced 'removal' and 're-provision' of the on state form of rsTagRFP as an acceptor.[159]

In Dreiklang, reversible photoswitching is not based on chromophore isomerization.[131] Instead, the imidazolinone ring of the *cis* chromophore undergoes a reversible hydration/dehydration reaction that is driven by light. On and off switching are achieved by using illumination wavelengths at ~365 and ~405 nm, respectively. Notably, different from all other known photoswitchers, the excitation of green fluorescence at ~515 nm is entirely decoupled from photoactivation in this variant.

### 3.4 Reversible and irreversible photoactivation in combination

IrisFP has been the first FP to feature both reversible and irreversible photoactivation (Fig. 4).[134] As for its parental protein, EosFP, intense irradiation of IrisFP with ~400 nm light induces irreversible photoconversion from the green to the red form (Fig. 4).[126] In addition, IrisFP exhibits reversible photoswitching in either form. This unique combination of photoactivation modes, which has been preserved in the monomeric variant, mIrisFP,[153] enables entirely new experimental schemes, for example, pulse-chase imaging combined with super-resolution localization microscopy (Fig. 6).[153] Feasibility of this approach was shown with a fusion of mIrisFP with paxillin, a protein involved in the formation of focal adhesions, by which cells adhere to the underlying surface. Focal adhesions were first imaged *via* reversible switching of the green form of mIrisFP in the fusion construct (Fig. 6a). Subsequently, focal adhesions in a subregion of the cell were tagged by using a brief 405 nm laser pulse, converting mIrisFP to its red form. Paxillin removal from disintegrating focal adhesions and incorporation into newly formed ones was observed with super-resolution by using reversible photoswitching of the red-converted species (Fig. 6b). Recently, a second member of this group of PA-FPs has been reported, NijiFP.[128] It was obtained from Dendra2[116] by introducing the same point mutation that had earlier transformed EosFP into IrisFP.[134]

### 3.5 Photoactivation and imaging strategies with high spatial and temporal resolution

Photoactivation is essential for the novel, fluorescence-based imaging strategies yielding high spatial and temporal resolution, notably pulse-chase imaging and super-resolution microscopy. In a pulse-chase experiment, which is often performed using a green-to-red photoconvertible FP, a certain subfraction of the initially green fluorescent fluorophores is tagged, *i.e.*, photoconverted to the red fluorescent state. Subsequently, the dynamics of this subpopulation can be monitored in real time even in the presence of many other fluorescent markers because they still emit at the initial wavelength and, therefore, their emission is not recorded.[28,47,114,118,153] Additional expression of (green-emitting) FPs during data collection on live cells also does not affect the outcome of the experiment.

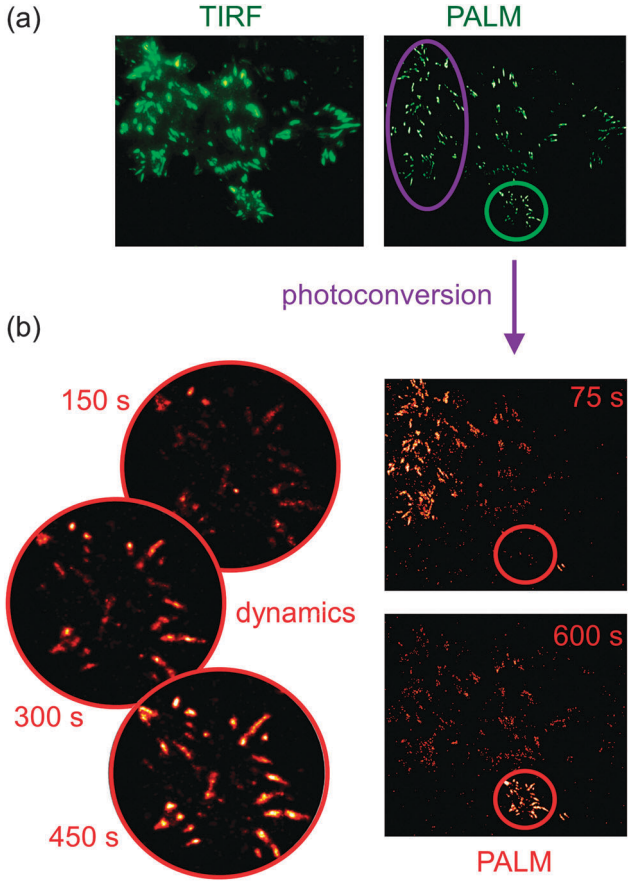


Fig. 6 Pulse-chase imaging with super-resolution. (a) TIRF and PALM images of a paxillin–mIrisFP fusion expressed in live HeLa (green emission). Paxillin is a platform protein involved in the formation of focal adhesion complexes. (b) PALM images of the activated paxillin–mIrisFP fusion construct (red emission) after photoconversion of a subpopulation (marked by the violet oval in panel a), are recorded as a function of time. On the right, the entire cell is shown 75 and 600 s after photoconversion. Paxillin molecules from the photoactivated subpopulation are observed to form new focal adhesions in the region marked by the red circles. On the left, close-ups of this region are shown for times 150, 300 and 450 s after photoconversion.

The super-resolution microscopy approaches developed in recent years circumvent the diffraction limit because the emission of neighboring fluorophores is not recorded simultaneously but sequentially in time by switching the fluorophores between their on and off states (see Section 5).

# 4. Essential properties of FPs for live-cell imaging

The color diversity of FPs extends over essentially the entire visible spectrum (see Tables 1–3). Structural, photophysical and photochemical properties of many FPs have been described in several excellent reviews.[25–28,67,96,160,161] Of utmost importance for any fluorescence marker is a high molecular brightness, so that it is well detectable in the presence of the unavoidable background, and a high photostability, so that it can endure many excitation–deexcitation cycles prior to photobleaching. Moreover, it should be conveniently excitable with commonly available (laser) sources. Red-shifted variants are generally preferred in experiments with live tissues and organisms because of the lower phototoxicity and increased penetration depth of the excitation light and reduced scattering of the emitted light. Moreover, red emission can readily be separated from the autofluorescence of biological samples in the green spectral region. In the following, we will dwell on those characteristics that are essential for live-cell imaging.

## 4.1 FP folding and chromophore maturation

When expressing FPs in live cells, the observed fluorescence intensity does not only depend on the molecular brightness of the FPs but also on the amount of FP molecules expressed in their functional form. The expression level depends on parameters such as transcription and translation efficiency, mRNA and protein stability, protein folding and chromophore maturation efficiency, and turnover of functional FPs in a live cell. The binding affinity of an FP fusion construct to its target site and the density of sites are also important.

GFP-like proteins only become fluorescent after the polypeptide chain has properly folded and the chromophore has matured. In fusion constructs, the folding efficiency can be compromised if the polypeptide linker that connects the FP to the partner protein is too short. Then, it is advisable to extend the polypeptide linker joining the two domains or, if feasible, exchange their order (N-terminal *versus* C-terminal fusion of the FP). Over the past few years, FP variants with enhanced folding robustness have been presented. Superfolder GFP, for instance, folds reliably and fast even when fused to poorly folded polypeptides;[162] the folding rate of 'superfast GFP' even exceeds that of superfolder GFP.[163]

Maturation of the chromophore may take from minutes to hours or even days. It needs to be sufficiently fast to allow the biological process to be followed. Half-lives of 1–2 h are often sufficient to label cells, organelles or proteins and to perform quantitative experiments. Very fast chromophore maturation is important for observing early promoter activity or studying individual translational events.[164] One also has to keep in mind that, in a live cell, there is a continuous turnover of FPs,[165] which makes the analysis of their spatio-temporal expression patterns or turn-over rates with conventional FPs virtually impossible. For such applications, photoconvertible FPs[160] or FPs with time-dependent spectral properties such as the fluorescent timer proteins[166] have proven useful. If FPs are used as donor–acceptor pairs in FRET measurements in living cells,[167–171] different maturation rates can have significant effects on the observed FRET signal. We also note that RFPs may have blue-shifted precursors during maturation,[172] which can also cause problems in FRET applications.

## 4.2 Oligomerization and cytotoxicity

For a wide range of applications, including monitoring of promoter and gene activity and highlighting of cellular organelles, cells and tissues, the oligomeric nature of an FP is entirely irrelevant.[109,173–175] Oligomerization or aggregation of FPs can,

 

however, have severe adverse effects. For example, wild-type copGFP has been observed to form huge, needle-like crystals inside eukaryotic cells and, thereby, destroying them within hours.[176] Other FPs tend to accumulate in lysosomes,[177] which can merge and become potentially cytotoxic agglomerates. In studies involving FP fusions with other proteins, oligomerization often interferes with the function of the fusion partner.[28] Formation of dimers or higher-order oligomers may be induced by the FP domain of the fusion construct and produce atypical localization or alter the normal function of the fusion partner. Moreover, if the protein of interest is also oligomeric, a network of interacting proteins may develop and cause cytotoxicity.

### 4.3 Photostability

Essentially all applications of FPs involve fluorescence measurements, so photostability is a key parameter, especially for long-term data acquisition, detection of weak fluorescence signals and quantitative measurements such as those based on FRET. Typically, the chromophore emits $10^4$–$10^6$ photons prior to experiencing permanent photodestruction.[153] The photostability of an FP inside a living cell may differ significantly from the one determined *in vitro*. Parameters such as intensity, time structure (pulsed *versus* continuous wave), and wavelength of the excitation light also affect the photophysical behavior.[178] Unfortunately, the relation between protein structure and photostability is hitherto only poorly understood so a rational approach toward higher photostability is still not viable.

### 4.4 Phototoxicity

Under illumination, FPs produce toxic reactive oxygen species (ROS) including singlet oxygen, $^1O_2$, which attack aromatic and sulfur-containing amino acids as well as cofactors of proteins.[179] The phototoxicity of typical FPs is low and can be ignored for most applications, which does not surprise considering that FPs evolved in organisms exposed to $O_2$ and plenty of sunlight. The β-can screens the chromophore efficiently from $O_2$ and prevents ROS generation. In the engineered FP KillerRed,[180] however, diffusion of $O_2$ towards the chromophore is facilitated by a water-filled channel. Therefore, KillerRed is orders of magnitude more phototoxic than avGFP and can be used as a genetically encoded photosensitizer, *e.g.*, for precise inactivation of selected proteins using the chromophore-assisted light inactivation (CALI) technique and for the targeted killing of cells, for example, in photodynamic therapy.[181]

### 4.5 Dynamic range

Fluorescence markers should provide a high contrast, so that the ratio between the desired fluorescence signal and the unwanted background is maximized. When using photoactivatable fluorophores, photoactivated FP molecules must be separable from the background produced by the residual emission of a large number of deactivated FPs. To achieve optimal contrast, the emission probability of emitting photons while in the dark state should be minimal and the one in the bright state should be high. In this context, by 'dark' we mean 'non-emitting into the detection channel'.

A higher dynamic range, *i.e.*, a higher contrast between the fluorescence emission of the photoactivated and deactivated forms, can be achieved with photoconvertible FPs than with photoswitchers. Photoconversion involves a permanent photochemical modification, whereas reversible photoswitching relies on a light-induced shift of the thermodynamic equilibrium between a bright and a dark state, the extent of which is limited and depends on the light wavelengths used (see Section 3.3).

## 5. FPs in super-resolution imaging

During the past decade, innovative super-resolution fluorescence microscopy techniques have been developed that offer the possibility to visualize the distribution, dynamics, and interactions of individual molecules with a spatial resolution down to ~10 nm, so that biological processes in live cells can be followed in time and space. Numerous reviews on biological applications[10,14,16–18,182–187] have borne witness to the huge impact that these novel techniques have in the life sciences. All these approaches rely on fluorophores that can alternate between an 'on' and an 'off' state. Instead of detecting the emission from fluorophores that are closer in distance than the diffraction limit of ~200 nm simultaneously, switching allows a sequential detection. The fluctuation approach, utilized in super-resolution optical fluctuation imaging (SOFI), is based on the statistical analysis of spatio-temporal fluctuations, *i.e.*, the blinking of fluorophores (typically quantum dots), to obtain subdiffraction optical resolution in all three dimensions. For further details, we refer to ref. 11, 12 and 188.

In the targeted approach to super-resolution, the sample is scanned with a certain spatial light intensity distribution pattern, which switches the fluorescent markers such that only a minor fraction, located in a region of sub-diffraction extension, is either in the on or off state. In STED microscopy, which is a particular realization of the RESOLFT technique,[4,189] the sample is raster-scanned by an excitation spot ('Airy disk') generated by tightly focused light, which locally induces electronic excitation of the fluorophores.[3] A second, toroidal (doughnut-shaped) intensity profile with zero intensity in its center is overlaid with the Airy spot (Fig. 7). The wavelength of this high-power depletion (STED) beam is red-shifted from the excitation beam so as to return all fluorophores to the ground state by stimulated emission except for those molecules in a small sub-wavelength region in the center of the Airy spot ('effective excitation', Fig. 7). To minimize re-excitation by the depletion beam, a large Stokes shift is advantageous. Stimulated emission is a fundamental physical property of all fluorophores; therefore, in principle, any fluorescent probe is suitable for STED microscopy. However, because typical fluorescence lifetimes are on the order of a few nanoseconds and depletion has to occur faster than emission, high laser powers of typically ~5 MW $cm^{-2}$ are needed for the STED beam. The image is built up by scanning the illumination patterns across the sample with a step size smaller than half the desired resolution.[190] Thus, a particular fluorophore is excited and deexcited many times as the Airy and depletion spots are

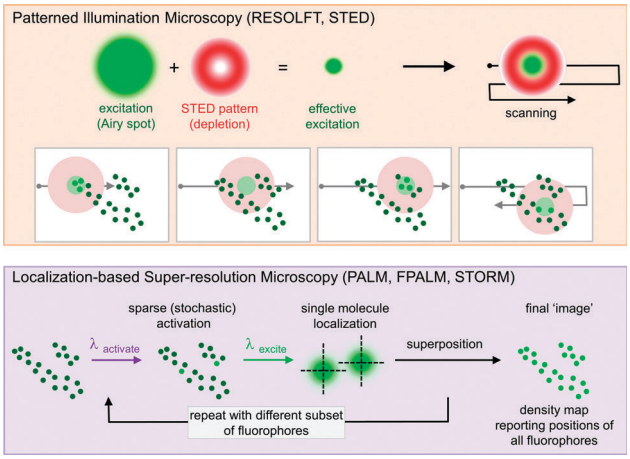


Fig. 7 Basic principles of super-resolution fluorescence microscopy techniques. The patterned illumination approach is based on the reduction of the effective excitation region. The sample is scanned by a tightly focused circular excitation beam. A second, overlapping doughnut-shaped laser beam deexcites all fluorophores except for those in the center. In the localization-based approach, only a few molecules are activated at any point in time and localized with high precision. The final 'image' is a density map of all fluorophore positions.

moved in suitably small steps across the sample. Consequently, excellent photostability is required for the markers. Compared with synthetic dyes, FPs have relatively poor photostability, so they have only sporadically been used for STED.[184,191–193]

However, RESOLFT microscopy can be performed with very low depletion beam intensities compatible with FPs. PS-FPs inherently feature long-lived on and off states. They can be switched selectively back and forth between these states many times by laser irradiation. Spontaneous transitions between the active and inactive forms occur with fairly low probabilities and, therefore, depletion of the active state (*via* photoswitching) requires orders of magnitude lower depletion laser intensities than when using STED. By using the red PS-FP asFP595, super-resolution RESOLFT imaging was performed with a depletion beam intensity of $<1$ kW cm$^{-2}$.[4]

In the localization approach to super-resolution, developed independently by three groups (photoactivation localization microscopy, PALM;[9] fluorescence photoactivation localization microscopy, FPALM;[7] stochastic optical reconstruction microscopy, STORM[8]), individual molecules are randomly photoactivated, *i.e.*, switched to the fluorescent state (on), while the surrounding molecules remain in the dark (off) state, so that the positions of these few individual emitters can be determined with high precision (Fig. 7). After photobleaching of these fluorophores, a new subset is activated and the positions are recorded again. The activation and localization steps are repeated, until the population of single activated molecules becomes negligible even at high laser powers ($10^2$–$10^4$ times). The final, high-resolution 'image' is, in fact, a density map showing the positions of all detected fluorophores (Fig. 7). Although precise molecular localization is computationally very demanding, image reconstruction can be performed online by using efficient algorithms and massively parallelized computation.[194–197]

### 5.1 FPs in patterned illumination-based super-resolution techniques

The RESOLFT approach requires reversible switching of PS-FPs. In the following, we discuss the illumination schemes for both positively and negatively charged PS-FPs emitting in the green, assuming that the *cis* and *trans* chromophores have p$K$ values as displayed in Fig. 5a and f.

Positive photoswitchers are typically non-fluorescent in the ground state, with most chromophores residing in the $T^-$ configuration (compare Section 3.3). To acquire a subdiffraction image, the sample is first 'reset', *i.e.*, $T^-$ is photoactivated by $\sim$480 nm light and isomerizes/protonates to yield non-fluorescent $C^H$ ($T^- \rightarrow C^H$, Fig. 8). Then, the chromophores in the periphery of the Airy spot are exposed to depletion light, so that $C^H \rightarrow T^-$ (dump, $\sim$400 nm). In the center, $C^H$ chromophores will be enhanced and restore the protonation equilibrium of the *cis* conformation, which causes a net production of fluorescent $C^-$ molecules. These are subsequently imaged by the probe beam (probe, $\sim$480 nm). It is readily apparent from Fig. 8 that this illumination scheme requires only two beams, the diffraction-limited switching/photoexcitation beam and the doughnut-shaped depletion beam. In practice, the sample can be scanned simultaneously with both beams. The concurrent on-switching and photoexcitation is advantageous as it speeds up image acquisition.

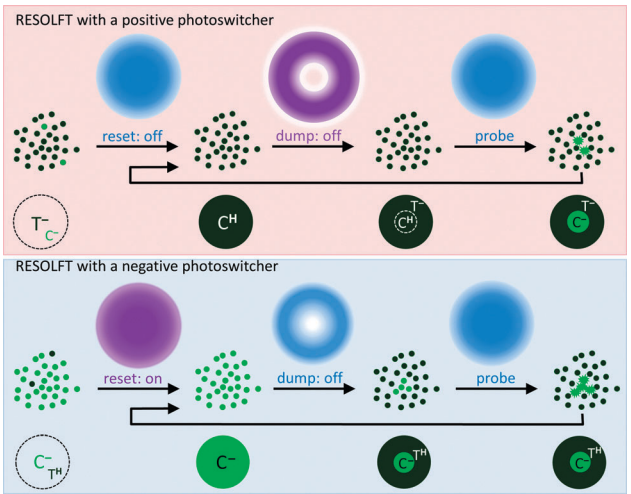


Fig. 8 Illumination schemes applied in RESOLFT microscopy. Active and non-active fluorophores in the sample are represented by bright green and dark green spots, respectively. Positive photoswitchers are typically non-fluorescent in thermal equilibrium, with most chromophores in $T^-$. First, the sample is 'reset': $T^-$ is photoactivated by $\sim$480 nm light and isomerizes/protonates to non-fluorescent $C^H$. Then, $C^H$ in the periphery of the Airy spot is exposed to depletion light, so that $C^H \rightarrow T^-$ (dump, $\sim$400 nm). $C^H$ in the center will restore the protonation equilibrium of the *cis* conformation, which causes a net production of fluorescent $C^-$ molecules. $C^-$ is imaged by the probe beam ($\sim$480 nm). Negative photoswitchers are first switched on by a $\sim$400 nm pulse of activating light (reset, $T^H \rightarrow C^-$). The depletion beam ($\sim$480 nm) switches off all fluorophores in the periphery (dump, $C^- \rightarrow T^H$). $C^-$ can be probed by a short pulse of $\sim$480 nm excitation light (probe). Depletion and probe beam have the same wavelength, but their beam profiles and intensities differ.

Negative photoswitchers call for a more elaborate illumination scheme. In the reset-dump-probe scheme, the FPs are first switched on by a ~400 nm pulse of activating light (reset, $T^H \rightarrow C^-$, Fig. 8). Then, the doughnut-shaped depletion beam is applied at the off-switching wavelength (~480 nm), switching off all fluorophores in the periphery (dump, $C^- \rightarrow T^H$). Only molecules in the center of the depletion beam remain fluorescent and can be probed by a short pulse of ~480 nm excitation light (probe). Note that the depletion and the probe beams have the same wavelength, but their beam profiles and intensities differ so that three illumination steps are required. The repetition rate of this sequence and, therefore, the scan speed is governed by the transition rates between the on and off states. In most negative photoswitchers, off-switching with blue light is 2–3 orders of magnitude slower than on-switching with violet light of comparable intensity,[158] rendering off-switching the time-limiting step in RESOLFT microscopy.

RESOLFT is a raster scanning technique, so a higher spatial resolution requires a smaller step size, which increases the number of excitation–depletion cycles experienced by an individual fluorophore accordingly. For a two-dimensional image scan, a ten-fold improvement over the diffraction-limited resolution requires roughly a ~100-fold increase in pixel number.[198] Therefore, RESOLFT critically relies on PS-FPs with a low switching fatigue. Switching fatigue refers to the number of on–off cycles that a PS-FP can perform prior to photodestruction and is closely connected to the switching kinetics. If the QY for photoswitching is high, the FP will emit only a few photons in each on phase. Therefore, it may go through several hundred or even thousand photoswitching cycles before it is permanently bleached. rsEGFP2, for example, was reported to be able to perform ~2100 cycles before the fluorescence intensity has decayed to 50% of its initial value.[158]

Especially for negative photoswitchers, a high photostability is desirable because, in every cycle, they are photoexcited by the dump beam and emit photons until deactivation occurs. Evidently, smaller step sizes also lead to slower image acquisition. In contrast to localization microscopy, however, the molecular brightness of the individual fluorophore is less crucial in RESOLFT because it is not a single-molecule technique; more than one molecule is typically imaged at each pixel provided that the labeling densities are sufficiently high.

We only briefly mention structured illumination microscopy (SIM),[199] which uses patterned illumination in the form of stripes to excite the sample rather than a point-like pattern as in STED/RESOLFT. Super-resolution is achieved by using high excitation intensity so that the fluorescence emission becomes saturated (saturated SIM, SSIM).[5,6] Thereby, sharp dark regions are created near the illumination pattern intensity zeros. Because the fluorophores have to be maintained in the vulnerable excited state for most of the time, SSIM requires very high excitation intensities when using normal fluorescence transitions. As with RESOLFT, the intensities required can, however, be reduced dramatically when employing PS-FPs.[200]

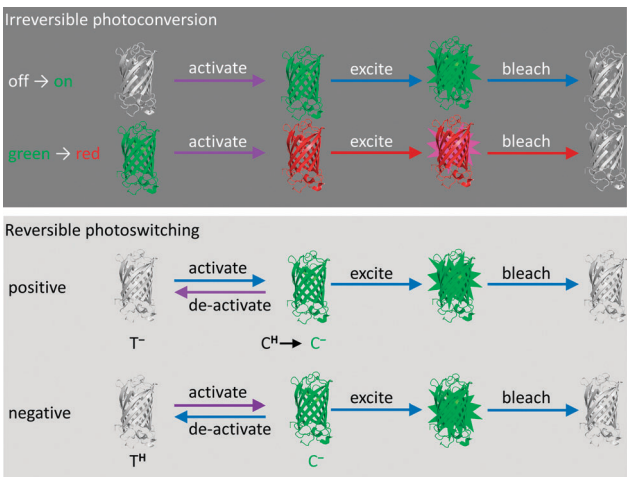


Fig. 9 Illumination schemes applied in PALM microscopy. Photoconvertible FPs expressed in the non-fluorescent off state are first activated (*e.g.*, with ~400 nm) and then probed (PA-GFP: ~480 nm). Green-to-red photoconvertible FPs are expressed in the deactivated state, which is emitting green fluorescence. The light used for photoconversion (~400 nm) is well separated in wavelength from that exciting the green (~480 nm) and red (532 nm) fluorophores. For localization microscopy with reversibly photoactivatable FPs, the absorption bands of the bright and dark species should be well separated so that each species can be targeted with high specificity. Before imaging, negative photoswitchers have to be activated (switched on) (green PS-FPs: ~400 nm, red PS-FPs: ~470 nm). With ~480 nm (~560 nm) light, green (red) PS-FPs are probed and also switched off. Positive photoswitchers are switched on by the excitation light (~480 nm for green PS-FPs, ~560 nm for red PS-FPs) and can be imaged concurrently until they bleach.

### 5.2 FPs in localization-based super-resolution techniques

Localization-based microscopy is inherently a single molecule technique (Fig. 7). From a large pool of photoactivatable markers, individual molecules are localized after stochastic photoactivation, while the majority of them are maintained in the off state. The ultimate resolution depends on (i) the localization precision and (ii) on the labeling density.

(i) If the fluorescent background is negligible, the localization precision scales roughly with the inverse square root of the number of photons collected from a single fluorophore.[201] In theory, the localization uncertainty amounts to ±5 nm upon detection of ~1000 photons. The uncertainty increases to ±15 nm with only ~100 photons collected from a particular fluorophore. In practice, detection of at least 100 photons per single fluorophore is desirable and often sufficient. FPs selected for localization-based techniques should have a high molecular brightness to emit a strong single-molecule signal above the background.[202] An excellent photostability ensures that a large number of photons can be detected per molecule before it photobleaches. Photoconvertible FPs undergo only a single activation step before registration and, therefore, are ideal for localization-based super-resolution microscopy. However, additional dark states may exist and create problems. It was recently shown that a significant fraction of photoactivated mEos2 actually undergoes multiple activation–deactivation cycles to long-lived dark states, which may lead to multiple counts of the same molecule and thus can give rise to errors.[203] In contrast, PS-FPs with negative photoswitching may

generate several temporally separated photon 'bursts' visible in different frames because they may be switched off by the excitation light.

(ii) The Nyquist–Shannon sampling theorem states that the distance between neighboring localized fluorophores must not be more than half the desired resolution.[190] Consequently, for a resolution of 10 nm, fluorophore densities of ~1000 per diffraction-limited spot (diameter ~200 nm) are required. Their residual fluorescence in the deactivated state has to be very low so as to not obscure the emission from an individual photoactivated FP within this pool. Therefore, a high dynamic range, *i.e.*, a high contrast between the fluorescence emission of the photoactivated and deactivated form of the FP, is of crucial importance.

In view of these considerations, photoconvertible FPs expressed in a non-fluorescent off state, *e.g.*, PA-GFP, appear to be optimal candidates. However, they are invisible prior to photoactivation and, thus, cannot be targeted selectively in the dark state (Fig. 9). These FPs may also be activated inadvertently by the excitation laser. Green-to-red photoconvertible FPs such as EosFP are, at present, the optimal choice. They are also expressed in the deactivated state, which, however, emits green fluorescence (Fig. 9). The light used for photoconversion (~400 nm) is well separated in wavelength from that exciting the green (~480 nm) and red (532 nm) fluorophores, so the risk of unintended photoconversion is greatly reduced. Locating these FPs in the cell prior to photoactivation is straightforward because of their green emission. For localization microscopy with reversibly photoactivatable FPs, the absorption bands of the bright and dark species should be well separated so that each species can be targeted with high specificity so as to minimize undesired photoactivation. Spontaneous thermally activated transitions between bright and dark states can occur, so sufficient longevity of the chromophore states ensures that photoactivation is entirely under light control. Negative photoswitchers yield the highest contrast for $pK_{cis} \ll pH_{sample} \ll pK_{trans}$, assuming that the anionic *cis* form is the fluorescent species (Fig. 5a). The laser that excites the fluorescence also switches the chromophore off and causes permanent photobleaching (Fig. 9). PS-FPs with a low quantum yield for off-switching are preferred because they emit their photons in one burst prior to photobleaching, which yields a high localization precision.[204] For all positive photoswitchers hitherto known, the non-fluorescent anionic *trans* isomer is the thermodynamically stable chromophore (see Section 3.3). Therefore, the majority of these FPs are initially in the dark state. They are switched on by the excitation light and can be imaged concurrently until they bleach (Fig. 9). These positive photoswitchers work essentially only in a pH region for which $pK_{cis} \approx pH \gg pK_{trans}$ (Fig. 5f).

Regardless of the activation mechanism, activation and deactivation should be properly adjusted by using suitable laser intensities. The time required for photoactivation to occur is governed by the product of laser intensity, absorption cross section and the QY of the photoreaction. Photoconvertible FPs are activated and read out only once before they are photobleached, yielding a single recorded localization event per molecule (disregarding complications due to additional dark states, *e.g.*, triplet states). The time resolution in localization-based super-resolution live-cell imaging with photoconvertible FPs can be controlled by varying the laser powers. The intensity of the photoactivating light is adjusted so as to record a suitable number of FPs per camera frame, and a high power of the read-out laser ensures that photobleaching occurs quickly, so that the next subset of fluorophores can be activated.

### 5.3 Conclusions

During the past decade, super-resolution techniques have been devised and implemented in optical microscopes that ingeniously circumvent the Abbe diffraction barrier. Recently, these techniques have also been combined with quantitative methods established to observe fast molecular motions, such as fluorescence correlation spectroscopy[205] and raster image correlation spectroscopy.[206] All these different approaches will be helpful and complement each other in unraveling the molecular details underlying biological processes in living matter. Progress in the field crucially hinges on further advances in fluorescent marker technology, however. For live-cell imaging with super-resolution, FPs are indispensable for the reason of being genetically encodable, which greatly simplifies assay development. The development of brighter, more photostable FPs will be beneficial for many applications. However, specific applications call for specific FPs and require careful selection; a one-fits-all FP suitable for every purpose is not within reach.

## Abbreviations

| | |
|---|---|
| avGFP | *Aequorea victoria* GFP |
| ECFP | Enhanced cyan fluorescent protein |
| EGFP | Enhanced green fluorescent protein |
| FP | Fluorescent protein |
| FRET | Förster resonance energy transfer |
| GFP | Green fluorescent protein |
| PA-GFP | Photoactivatable GFP |
| PA-FP | Photoactivatable FP |
| PAm | Photoactivatable monomeric |
| PALM | Photoactivation localization microscopy |
| PALMIRA | PALM with independently running acquisition |
| PS-FP | Photoswitchable FP |
| QY | Quantum yield |
| RESOLFT | Reversible saturable optical fluorescence transitions microscopy |
| RFP | Red fluorescent protein |
| ROS | Reactive oxygen species |
| SIM | Structured illumination microscopy |
| SSIM | Saturated SIM |
| STED | Stimulated emission depletion |
| STORM | Stochastical optical reconstruction microscopy |

## Acknowledgements

This work was supported by the Deutsche Forschungsgemeinschaft (DFG) and the State of Baden-Württemberg through the Center for Functional Nanostructures (CFN) and by DFG grant Ni 291/9.

 

## References


1 E. Abbe, *Arch. Mikrosk. Anat. Entwicklungsmech.*, 1873, **9**, 413–468.
2 S. W. Hell, *Science*, 2007, **316**, 1153–1158.
3 S. W. Hell and J. Wichmann, *Opt. Lett.*, 1994, **19**, 780–782.
4 M. Hofmann, C. Eggeling, S. Jakobs and S. W. Hell, *Proc. Natl. Acad. Sci. U. S. A.*, 2005, **102**, 17565–17569.
5 M. G. Gustafsson, *Proc. Natl. Acad. Sci. U. S. A.*, 2005, **102**, 13081–13086.
6 R. Heintzmann and M. G. Gustafsson, *Nat. Photonics*, 2009, **3**, 362–364.
7 S. T. Hess, T. P. Girirajan and M. D. Mason, *Biophys. J.*, 2006, **91**, 4258–4272.
8 M. J. Rust, M. Bates and X. Zhuang, *Nat. Methods*, 2006, **3**, 793–795.
9 E. Betzig, G. H. Patterson, R. Sougrat, O. W. Lindwasser, S. Olenych, J. S. Bonifacino, M. W. Davidson, J. Lippincott-Schwartz and H. F. Hess, *Science*, 2006, **313**, 1642–1645.
10 P. Sengupta, S. Van Engelenburg and J. Lippincott-Schwartz, *Dev. Cell*, 2012, **23**, 1092–1102.
11 T. Dertinger, R. Colyer, G. Iyer, S. Weiss and J. Enderlein, *Proc. Natl. Acad. Sci. U. S. A.*, 2009, **106**, 22287–22292.
12 S. Geissbuehler, N. L. Bocchio, C. Dellagiacoma, C. Berclaz, M. Leutenegger and T. Lasser, *Opt. Nanoscopy*, 2012, **1**, 4.
13 P. N. Hedde and G. U. Nienhaus, *Biophys. Rev.*, 2010, **2**, 147–158.
14 B. Huang, *Curr. Opin. Chem. Biol.*, 2010, **14**, 10–14.
15 B. Huang, H. Babcock and X. Zhuang, *Cell*, 2010, **143**, 1047–1058.
16 B. Huang, M. Bates and X. Zhuang, *Annu. Rev. Biochem.*, 2009, **78**, 993–1016.
17 L. Schermelleh, R. Heintzmann and H. Leonhardt, *J. Cell Biol.*, 2010, **190**, 165–175.
18 D. Toomre and J. Bewersdorf, *Annu. Rev. Cell Dev. Biol.*, 2010, **26**, 285–314.
19 G. T. Dempsey, J. C. Vaughan, K. H. Chen, M. Bates and X. Zhuang, *Nat. Methods*, 2011, **8**, 1027–1036.
20 J. Fan and P. K. Chu, *Small*, 2010, **6**, 2080–2098.
21 C. C. Fu, H. Y. Lee, K. Chen, T. S. Lim, H. Y. Wu, P. K. Lin, P. K. Wei, P. H. Tsao, H. C. Chang and W. Fann, *Proc. Natl. Acad. Sci. U. S. A.*, 2007, **104**, 727–732.
22 X. Michalet, F. F. Pinaud, L. A. Bentolila, J. M. Tsay, S. Doose, J. J. Li, G. Sundaresan, A. M. Wu, S. S. Gambhir and S. Weiss, *Science*, 2005, **307**, 538–544.
23 L. Shang, S. Dong and G. U. Nienhaus, *Nano Today*, 2011, **6**, 401–418.
24 L. Shang and G. U. Nienhaus, *Mater. Today*, 2013, **16**, 58–66.
25 N. C. Shaner, P. A. Steinbach and R. Y. Tsien, *Nat. Methods*, 2005, **2**, 905–909.
26 D. M. Chudakov, S. Lukyanov and K. A. Lukyanov, *Trends Biotechnol.*, 2005, **23**, 605–613.
27 R. N. Day and M. W. Davidson, *Chem. Soc. Rev.*, 2009, **38**, 2887–2921.
28 J. Wiedenmann, F. Oswald and G. U. Nienhaus, *IUBMB Life*, 2009, **61**, 1029–1042.
29 V. T. Oi, A. N. Glazer and L. Stryer, *J. Cell Biol.*, 1982, **93**, 981–986.
30 X. Shu, A. Royant, M. Z. Lin, T. A. Aguilera, V. Lev-Ram, P. A. Steinbach and R. Y. Tsien, *Science*, 2009, **324**, 804–807.
31 A. Kumagai, R. Ando, H. Miyatake, P. Greimel, T. Kobayashi, Y. Hirabayashi, T. Shimogori and A. Miyawaki, *Cell*, 2013, **153**, 1602–1611.
32 O. Shimomura, F. H. Johnson and Y. Saiga, *J. Cell. Comp. Physiol.*, 1962, **59**, 223–239.
33 D. C. Prasher, V. K. Eckenrode, W. W. Ward, F. G. Prendergast and M. J. Cormier, *Gene*, 1992, **111**, 229–233.
34 M. Chalfie, Y. Tu, G. Euskirchen, W. W. Ward and D. C. Prasher, *Science*, 1994, **263**, 802–805.
35 R. Y. Tsien, *Annu. Rev. Biochem.*, 1998, **67**, 509–544.
36 G. U. Nienhaus, *Angew. Chem., Int. Ed.*, 2008, **47**, 8992–8994.
37 M. Zimmer, *Chem. Soc. Rev.*, 2009, **38**, 2823–2832.
38 R. F. Service, *Science*, 2008, **322**, 361.
39 M. V. Matz, A. F. Fradkov, Y. A. Labas, A. P. Savitsky, A. G. Zaraisky, M. L. Markelov and S. A. Lukyanov, *Nat. Biotechnol.*, 1999, **17**, 969–973.
40 J. Wiedenmann, C. Elke, K. D. Spindler and W. Funke, *Proc. Natl. Acad. Sci. U. S. A.*, 2000, **97**, 14091–14096.
41 A. Miyawaki, *Cell Struct. Funct.*, 2002, **27**, 343–347.
42 G. S. Baird, D. A. Zacharias and R. Y. Tsien, *Proc. Natl. Acad. Sci. U. S. A.*, 2000, **97**, 11984–11989.
43 N. C. Shaner, R. E. Campbell, P. A. Steinbach, B. N. Giepmans, A. E. Palmer and R. Y. Tsien, *Nat. Biotechnol.*, 2004, **22**, 1567–1572.
44 F. Oswald, F. Schmitt, A. Leutenegger, S. Ivanchenko, C. D'Angelo, A. Salih, S. Maslakova, M. Bulina, R. Schirmbeck, G. U. Nienhaus, M. V. Matz and J. Wiedenmann, *FEBS J.*, 2007, **274**, 1102–1109.
45 J. Wiedenmann, S. Ivanchenko, F. Oswald and G. U. Nienhaus, *Mar. Biotechnol.*, 2004, **6**, 270–277.
46 V. V. Verkhusha and K. A. Lukyanov, *Nat. Biotechnol.*, 2004, **22**, 289–296.
47 J. Wiedenmann and G. U. Nienhaus, *Expert Rev. Proteomics*, 2006, **3**, 361–374.
48 R. Ando, H. Hama, M. Yamamoto-Hino, H. Mizuno and A. Miyawaki, *Proc. Natl. Acad. Sci. U. S. A.*, 2002, **99**, 12651–12656.
49 S. Habuchi, R. Ando, P. Dedecker, W. Verheijen, H. Mizuno, A. Miyawaki and J. Hofkens, *Proc. Natl. Acad. Sci. U. S. A.*, 2005, **102**, 9511–9516.
50 M. Wolff, J. Wiedenmann, G. U. Nienhaus, M. Valler and R. Heilker, *Drug Discovery Today*, 2006, **11**, 1054–1060.
51 C. Chakraborty, C. H. Hsu, Z. H. Wen and C. S. Lin, *Curr. Pharm. Des.*, 2009, **15**, 3552–3570.
52 M. W. Davidson and R. E. Campbell, *Nat. Methods*, 2009, **6**, 713–717.
53 M. Ormö, A. B. Cubitt, K. Kallio, L. A. Gross, R. Y. Tsien and S. J. Remington, *Science*, 1996, **273**, 1392–1395.

54 F. Yang, L. G. Moss and G. N. Phillips Jr, *Nat. Biotechnol.*, 1996, **14**, 1246–1251.
55 S. L. Maddalo and M. Zimmer, *Photochem. Photobiol.*, 2006, **82**, 367–372.
56 E. K. Bomati, G. Manning and D. D. Deheyn, *BMC Evol. Biol.*, 2009, **9**, 77.
57 O. V. Stepanenko, I. M. Kuznetsova, V. V. Verkhusha and K. K. Turoverov, *Int. Rev. Cell Mol. Biol.*, 2013, **302**, 221–278.
58 J. Wiedenmann, A. Schenk, C. Röcker, A. Girod, K. D. Spindler and G. U. Nienhaus, *Proc. Natl. Acad. Sci. U. S. A.*, 2002, **99**, 11646–11651.
59 S. J. Remington, R. M. Wachter, D. K. Yarbrough, B. Branchaud, D. C. Anderson, K. Kallio and K. A. Lukyanov, *Biochemistry*, 2005, **44**, 202–212.
60 X. Shu, N. C. Shaner, C. A. Yarbrough, R. Y. Tsien and S. J. Remington, *Biochemistry*, 2006, **45**, 9639–9646.
61 Y. G. Yanushevich, D. B. Staroverov, A. P. Savitsky, A. F. Fradkov, N. G. Gurskaya, M. E. Bulina, K. A. Lukyanov and S. A. Lukyanov, *FEBS Lett.*, 2002, **511**, 11–14.
62 A. M. Loening, T. D. Fenn and S. S. Gambhir, *J. Mol. Biol.*, 2007, **374**, 1017–1028.
63 D. A. Shagin, E. V. Barsova, Y. G. Yanushevich, A. F. Fradkov, K. A. Lukyanov, Y. A. Labas, T. N. Semenova, J. A. Ugalde, A. Meyers, J. M. Nunez, E. A. Widder, S. A. Lukyanov and M. V. Matz, *Mol. Biol. Evol.*, 2004, **21**, 841–850.
64 K. Nienhaus, F. Renzi, B. Vallone, J. Wiedenmann and G. U. Nienhaus, *Biophys. J.*, 2006, **91**, 4210–4220.
65 K. Brejc, T. K. Sixma, P. A. Kitts, S. R. Kain, R. Y. Tsien, M. Örmo and S. J. Remington, *Proc. Natl. Acad. Sci. U. S. A.*, 1997, **94**, 2306–2311.
66 C. Scharnagl, R. Raupp-Kossmann and S. F. Fischer, *Biophys. J.*, 1999, **77**, 1839–1857.
67 D. M. Chudakov, M. V. Matz, S. Lukyanov and K. A. Lukyanov, *Physiol. Rev.*, 2010, **90**, 1103–1163.
68 R. Bizzarri, M. Serresi, S. Luin and F. Beltram, *Anal. Bioanal. Chem.*, 2009, **393**, 1107–1122.
69 G. T. Hanson, T. B. McAnaney, E. S. Park, M. E. Rendell, D. K. Yarbrough, S. Chu, L. Xi, S. G. Boxer, M. H. Montrose and S. J. Remington, *Biochemistry*, 2002, **41**, 15477–15488.
70 S. Kredel, K. Nienhaus, M. Wolff, F. Oswald, S. Ivanchenko, F. Cymer, A. Jeromin, F. J. Michel, K.-D. Spindler, R. Heilker, G. U. Nienhaus and J. Wiedenmann, *Chem. Biol.*, 2008, **15**, 224–233.
71 S. Kredel, F. Oswald, K. Nienhaus, K. Deuschle, C. Röcker, M. Wolff, R. Heilker, G. U. Nienhaus and J. Wiedenmann, *PLoS One*, 2009, **4**, e4391.
72 J. Wiedenmann, B. Vallone, F. Renzi, K. Nienhaus, S. Ivanchenko, C. Röcker and G. U. Nienhaus, *J. Biomed. Opt.*, 2005, **10**, 014003.
73 F. V. Subach, G. H. Patterson, S. Manley, J. M. Gillette, J. Lippincott-Schwartz and V. V. Verkhusha, *Nat. Methods*, 2009, **6**, 153–159.
74 D. C. Loos, S. Habuchi, C. Flors, J. Hotta, J. Wiedenmann, G. U. Nienhaus and J. Hofkens, *J. Am. Chem. Soc.*, 2006, **128**, 6270–6271.
75 K. Nienhaus, H. Nar, R. Heilker, J. Wiedenmann and G. U. Nienhaus, *J. Am. Chem. Soc.*, 2008, **130**, 12578–12579.
76 M. Chattoraj, B. A. King, G. U. Bublitz and S. G. Boxer, *Proc. Natl. Acad. Sci. U. S. A.*, 1996, **93**, 8362–8367.
77 H. Lossau, A. Kummer, R. Heinecke, F. Pollinger-Dammer, C. Kompa, G. Bieser, T. Jonsson, C. M. Silva, M. M. Yang, D. C. Youvan and M. E. Michel-Beyerle, *Chem. Phys.*, 1996, **213**, 1–16.
78 M. A. Lill and V. Helms, *Proc. Natl. Acad. Sci. U. S. A.*, 2002, **99**, 2778–2781.
79 D. Stoner-Ma, A. A. Jaye, P. Matousek, M. Towrie, S. R. Meech and P. J. Tonge, *J. Am. Chem. Soc.*, 2005, **127**, 2864–2865.
80 G. U. Nienhaus, *ChemPhysChem*, 2010, **11**, 971–974.
81 C. Fang, R. R. Frontiera, R. Tran and R. A. Mathies, *Nature*, 2009, **462**, 200–204.
82 D. Stoner-Ma, A. A. Jaye, K. L. Ronayne, J. Nappa, P. J. Tonge and S. R. Meech, *Chem. Phys.*, 2008, **350**, 193–200.
83 X. Shu, P. Leiderman, R. Gepshtein, N. R. Smith, K. Kallio, D. Huppert and S. J. Remington, *Protein Sci.*, 2007, **16**, 2703–2710.
84 T. B. McAnaney, E. S. Park, G. T. Hanson, S. J. Remington and S. G. Boxer, *Biochemistry*, 2002, **41**, 15489–15494.
85 H. E. Seward and C. R. Bagshaw, *Chem. Soc. Rev.*, 2009, **38**, 2842–2851.
86 D. M. Shcherbakova, M. A. Hink, L. Joosen, T. W. Gadella and V. V. Verkhusha, *J. Am. Chem. Soc.*, 2012, **134**, 7913–7923.
87 K. D. Piatkevich, J. Hulit, O. M. Subach, B. Wu, A. Abdulla, J. E. Segall and V. V. Verkhusha, *Proc. Natl. Acad. Sci. U. S. A.*, 2010, **107**, 5369–5374.
88 K. D. Piatkevich, V. N. Malashkevich, S. C. Almo and V. V. Verkhusha, *J. Am. Chem. Soc.*, 2010, **132**, 10762–10770.
89 K. A. Lukyanov, D. M. Chudakov, S. Lukyanov and V. V. Verkhusha, *Nat. Rev. Mol. Cell Biol.*, 2005, **6**, 885–891.
90 S. Ivanchenko, S. Glaschick, C. Röcker, F. Oswald, J. Wiedenmann and G. U. Nienhaus, *Biophys. J.*, 2007, **92**, 4451–4457.
91 R. M. Dickson, A. B. Cubitt, R. Y. Tsien and W. E. Moerner, *Nature*, 1997, **388**, 355–358.
92 T. Ha and P. Tinnefeld, *Annu. Rev. Phys. Chem.*, 2012, **63**, 595–617.
93 A. Roy, M. J. Field, V. Adam and D. Bourgeois, *J. Am. Chem. Soc.*, 2011, **133**, 18586–18589.
94 C. Steinhauer, M. S. Itano and P. Tinnefeld, *Methods Mol. Biol.*, 2013, **950**, 111–129.
95 D. T. Burnette, P. Sengupta, Y. Dai, J. Lippincott-Schwartz and B. Kachar, *Proc. Natl. Acad. Sci. U. S. A.*, 2011, **108**, 21081–21086.
96 N. C. Shaner, G. H. Patterson and M. W. Davidson, *J. Cell Sci.*, 2007, **120**, 4247–4260.
97 G. H. Patterson and J. Lippincott-Schwartz, *Science*, 2002, **297**, 1873–1877.
98 J. N. Henderson, R. Gepshtein, J. R. Heenan, K. Kallio, D. Huppert and S. J. Remington, *J. Am. Chem. Soc.*, 2009, **131**, 4176–4177.

 

99 Y. Chen, P. J. MacDonald, J. P. Skinner, G. H. Patterson and J. D. Müller, *Microsc. Res. Tech.*, 2006, **69**, 220–226.
100 J. Martini, K. Schmied, R. Palmisano, K. Toensing, D. Anselmetti and T. Merkle, *J. Struct. Biol.*, 2007, **158**, 401–409.
101 T. Matsuda, A. Miyawaki and T. Nagai, *Nat. Methods*, 2008, **5**, 339–345.
102 M. Schneider, S. Barozzi, I. Testa, M. Faretta and A. Diaspro, *Biophys. J.*, 2005, **89**, 1346–1352.
103 R. E. Campbell, O. Tour, A. E. Palmer, P. A. Steinbach, G. S. Baird, D. A. Zacharias and R. Y. Tsien, *Proc. Natl. Acad. Sci. U. S. A.*, 2002, **99**, 7877–7882.
104 V. V. Verkhusha and A. Sorkin, *Chem. Biol.*, 2005, **12**, 279–285.
105 F. V. Subach, V. N. Malashkevich, W. D. Zencheck, H. Xiao, G. S. Filonov, S. C. Almo and V. V. Verkhusha, *Proc. Natl. Acad. Sci. U. S. A.*, 2009, **106**, 21097–21102.
106 E. M. Merzlyak, J. Goedhart, D. Shcherbo, M. E. Bulina, A. S. Shcheglov, A. F. Fradkov, A. Gaintzeva, K. A. Lukyanov, S. Lukyanov, T. W. Gadella and D. M. Chudakov, *Nat. Methods*, 2007, **4**, 555–557.
107 F. V. Subach, G. H. Patterson, M. Renz, J. Lippincott-Schwartz and V. V. Verkhusha, *J. Am. Chem. Soc.*, 2010, **132**, 6481–6491.
108 M. S. Gunewardene, F. V. Subach, T. J. Gould, G. P. Penoncello, M. V. Gudheti, V. V. Verkhusha and S. T. Hess, *Biophys. J.*, 2011, **101**, 1522–1528.
109 D. Shcherbo, E. M. Merzlyak, T. V. Chepurnykh, A. F. Fradkov, G. V. Ermakova, E. A. Solovieva, K. A. Lukyanov, E. A. Bogdanova, A. G. Zaraisky, S. Lukyanov and D. M. Chudakov, *Nat. Methods*, 2007, **4**, 741–746.
110 N. G. Gurskaya, A. F. Fradkov, N. I. Pounkova, D. B. Staroverov, M. E. Bulina, Y. G. Yanushevich, Y. A. Labas, S. Lukyanov and K. A. Lukyanov, *Biochem. J.*, 2003, **373**, 403–408.
111 D. M. Chudakov, V. V. Verkhusha, D. B. Staroverov, E. A. Souslova, S. Lukyanov and K. A. Lukyanov, *Nat. Biotechnol.*, 2004, **22**, 1435–1439.
112 D. M. Chudakov, S. Lukyanov and K. A. Lukyanov, *Nat. Protocols*, 2007, **2**, 2024–2032.
113 J. Wiedenmann, S. Ivanchenko, F. Oswald, F. Schmitt, C. Röcker, A. Salih, K. D. Spindler and G. U. Nienhaus, *Proc. Natl. Acad. Sci. U. S. A.*, 2004, **101**, 15905–15910.
114 G. U. Nienhaus, K. Nienhaus, A. Hölzle, S. Ivanchenko, F. Renzi, F. Oswald, M. Wolff, F. Schmitt, C. Röcker, B. Vallone, W. Weidemann, R. Heilker, H. Nar and J. Wiedenmann, *Photochem. Photobiol.*, 2006, **82**, 351–358.
115 N. G. Gurskaya, V. V. Verkhusha, A. S. Shcheglov, D. B. Staroverov, T. V. Chepurnykh, A. F. Fradkov, S. Lukyanov and K. A. Lukyanov, *Nat. Biotechnol.*, 2006, **24**, 461–465.
116 V. Adam, K. Nienhaus, D. Bourgeois and G. U. Nienhaus, *Biochemistry*, 2009, **48**, 4905–4915.
117 H. Tsutsui, S. Karasawa, H. Shimizu, N. Nukina and A. Miyawaki, *EMBO Rep.*, 2005, **6**, 233–238.
118 H. Hoi, N. C. Shaner, M. W. Davidson, C. W. Cairo, J. Wang and R. E. Campbell, *J. Mol. Biol.*, 2010, **401**, 776–791.
119 A. L. McEvoy, H. Hoi, M. Bates, E. Platonova, P. J. Cranfill, M. A. Baird, M. W. Davidson, H. Ewers, J. Liphardt and R. E. Campbell, *PLoS One*, 2012, **7**, e51314.
120 K. Nienhaus, G. U. Nienhaus, J. Wiedenmann and H. Nar, *Proc. Natl. Acad. Sci. U. S. A.*, 2005, **102**, 9156–9159.
121 I. Hayashi, H. Mizuno, K. I. Tong, T. Furuta, F. Tanaka, M. Yoshimura, A. Miyawaki and M. Ikura, *J. Mol. Biol.*, 2007, **372**, 918–926.
122 H. Tsutsui, H. Shimizu, H. Mizuno, N. Nukina, T. Furuta and A. Miyawaki, *Chem. Biol.*, 2009, **16**, 1140–1147.
123 M. Lelimousin, V. Adam, G. U. Nienhaus, D. Bourgeois and M. J. Field, *J. Am. Chem. Soc.*, 2009, **131**, 16814–16823.
124 J. Mathur, R. Radhamony, A. M. Sinclair, A. Donoso, N. Dunn, E. Roach, D. Radford, P. S. Mohaghegh, D. C. Logan, K. Kokolic and N. Mathur, *Plant Physiol. Biochem.*, 2010, **154**, 1573–1587.
125 S. A. McKinney, C. S. Murphy, K. L. Hazelwood, M. W. Davidson and L. L. Looger, *Nat. Methods*, 2009, **6**, 131–133.
126 J. Wiedenmann, S. Gayda, V. Adam, F. Oswald, K. Nienhaus, D. Bourgeois and G. U. Nienhaus, *J. Biophotonics*, 2011, **4**, 377–390.
127 M. Zhang, H. Chang, Y. Zhang, J. Yu, L. Wu, W. Ji, J. Chen, B. Liu, J. Lu, Y. Liu, J. Zhang, P. Xu and T. Xu, *Nat. Methods*, 2012, **9**, 727–729.
128 V. Adam, B. Moeyaert, C. C. David, H. Mizuno, M. Lelimousin, P. Dedecker, R. Ando, A. Miyawaki, J. Michiels, Y. Engelborghs and J. Hofkens, *Chem. Biol.*, 2011, **18**, 1241–1251.
129 S. Habuchi, H. Tsutsui, A. B. Kochaniak, A. Miyawaki and A. M. van Oijen, *PLoS One*, 2008, **3**, e3944.
130 O. M. Subach, G. H. Patterson, L. M. Ting, Y. Wang, J. S. Condeelis and V. V. Verkhusha, *Nat. Methods*, 2011, **8**, 771–777.
131 T. Brakemann, A. C. Stiel, G. Weber, M. Andresen, I. Testa, T. Grotjohann, M. Leutenegger, U. Plessmann, H. Urlaub, C. Eggeling, M. C. Wahl, S. W. Hell and S. Jakobs, *Nat. Biotechnol.*, 2011, **29**, 942–947.
132 M. Andresen, A. C. Stiel, S. Trowitzsch, G. Weber, C. Eggeling, M. C. Wahl, S. W. Hell and S. Jakobs, *Proc. Natl. Acad. Sci. U. S. A.*, 2007, **104**, 13005–13009.
133 J. N. Henderson, H. W. Ai, R. E. Campbell and S. J. Remington, *Proc. Natl. Acad. Sci. U. S. A.*, 2007, **104**, 6672–6677.
134 V. Adam, M. Lelimousin, S. Boehme, G. Desfonds, K. Nienhaus, M. J. Field, J. Wiedenmann, S. McSweeney, G. U. Nienhaus and D. Bourgeois, *Proc. Natl. Acad. Sci. U. S. A.*, 2008, **105**, 18343–18348.
135 S. Gayda, K. Nienhaus and G. U. Nienhaus, *Biophys. J.*, 2012, **103**, 2521–2531.
136 V. Voliani, R. Bizzarri, R. Nifosi, S. Abbruzzetti, E. Grandi, C. Viappiani and F. Beltram, *J. Phys. Chem. B*, 2008, **112**, 10714–10722.
137 D. M. Chudakov, A. V. Feofanov, N. N. Mudrik, S. Lukyanov and K. A. Lukyanov, *J. Biol. Chem.*, 2003, **278**, 7215–7219.

138 T. Brakemann, G. Weber, M. Andresen, G. Groenhof, A. C. Stiel, S. Trowitzsch, C. Eggeling, H. Grubmüller, S. W. Hell, M. C. Wahl and S. Jakobs, *J. Biol. Chem.*, 2010, **285**, 14603–14609.
139 S. Olsen, K. Lamothe and T. J. Martinez, *J. Am. Chem. Soc.*, 2010, **132**, 1192–1193.
140 A. C. Stiel, M. Andresen, H. Bock, M. Hilbert, J. Schilde, A. Schönle, C. Eggeling, A. Egner, S. W. Hell and S. Jakobs, *Biophys. J.*, 2008, **95**, 2989–2997.
141 C. Flors, J. Hotta, H. Uji-i, P. Dedecker, R. Ando, H. Mizuno, A. Miyawaki and J. Hofkens, *J. Am. Chem. Soc.*, 2007, **129**, 13970–13977.
142 X. Li, L. W. Chung, H. Mizuno, A. Miyawaki and K. Morokuma, *J. Phys. Chem. B*, 2010, **114**, 1114–1126.
143 R. Ando, H. Mizuno and A. Miyawaki, *Science*, 2004, **306**, 1370–1373.
144 H. Shroff, C. G. Galbraith, J. A. Galbraith, H. White, J. Gillette, S. Olenych, M. W. Davidson and E. Betzig, *Proc. Natl. Acad. Sci. U. S. A.*, 2007, **104**, 20308–20313.
145 P. Dedecker, J. Hotta, C. Flors, M. Sliwa, H. Uji-i, M. B. Roeffaers, R. Ando, H. Mizuno, A. Miyawaki and J. Hofkens, *J. Am. Chem. Soc.*, 2007, **129**, 16132–16141.
146 A. C. Stiel, S. Trowitzsch, G. Weber, M. Andresen, C. Eggeling, S. W. Hell, S. Jakobs and M. C. Wahl, *Biochem. J.*, 2007, **402**, 35–42.
147 H. Bock, C. Geisler, C. A. Wurm, C. von Middendorff, S. Jakobs, A. Schönle, A. Egner, S. W. Hell and C. Eggeling, *Appl. Phys. B: Lasers Opt.*, 2007, **88**, 161–165.
148 A. Egner, C. Geisler, C. von Middendorff, H. Bock, D. Wenzel, R. Medda, M. Andresen, A. C. Stiel, S. Jakobs, C. Eggeling, A. Schönle and S. W. Hell, *Biophys. J.*, 2007, **93**, 3285–3290.
149 M. Andresen, A. C. Stiel, J. Fölling, D. Wenzel, A. Schönle, A. Egner, C. Eggeling, S. W. Hell and S. Jakobs, *Nat. Biotechnol.*, 2008, **26**, 1035–1040.
150 A. R. Faro, P. Carpentier, G. Jonasson, G. Pompidor, D. Arcizet, I. Demachy and D. Bourgeois, *J. Am. Chem. Soc.*, 2011, **133**, 16362–16365.
151 M. Lummer, F. Humpert, M. Wiedenlubbert, M. Sauer, M. Schuttpelz and D. Staiger, *Mol. Plant*, 2013, DOI: 10.1093/mp/sst040.
152 H. Chang, M. Zhang, W. Ji, J. Chen, Y. Zhang, B. Liu, J. Lu, J. Zhang, P. Xu and T. Xu, *Proc. Natl. Acad. Sci. U. S. A.*, 2012, **109**, 4455–4460.
153 J. Fuchs, S. Böhme, F. Oswald, P. N. Hedde, M. Krause, J. Wiedenmann and G. U. Nienhaus, *Nat. Methods*, 2010, **7**, 627–630.
154 A. Brodehl, P. N. Hedde, M. Dieding, A. Fatima, V. Walhorn, S. Gayda, T. Saric, B. Klauke, J. Gummert, D. Anselmetti, M. Heilemann, G. U. Nienhaus and H. Milting, *J. Biol. Chem.*, 2012, **287**, 16047–16057.
155 R. Bizzarri, M. Serresi, F. Cardarelli, S. Abbruzzetti, B. Campanini, C. Viappiani and F. Beltram, *J. Am. Chem. Soc.*, 2010, **132**, 85–95.
156 T. Grotjohann, I. Testa, M. Leutenegger, H. Bock, N. T. Urban, F. Lavoie-Cardinal, K. I. Willig, C. Eggeling, S. Jakobs and S. W. Hell, *Nature*, 2011, **478**, 204–208.
157 B. P. Cormack, R. H. Valdivia and S. Falkow, *Gene*, 1996, **173**, 33–38.
158 T. Grotjohann, I. Testa, M. Reuss, T. Brakemann, C. Eggeling, S. W. Hell and S. Jakobs, *eLife*, 2012, **1**, e00248.
159 F. V. Subach, L. Zhang, T. W. Gadella, N. G. Gurskaya, K. A. Lukyanov and V. V. Verkhusha, *Chem. Biol.*, 2010, **17**, 745–755.
160 J. Lippincott-Schwartz and G. H. Patterson, *Science*, 2003, **300**, 87–91.
161 G. J. Kremers, S. G. Gilbert, P. J. Cranfill, M. W. Davidson and D. W. Piston, *J. Cell Sci.*, 2011, **124**, 157–160.
162 J. D. Pedelacq, S. Cabantous, T. Tran, T. C. Terwilliger and G. S. Waldo, *Nat. Biotechnol.*, 2006, **24**, 79–88.
163 A. C. Fisher and M. P. DeLisa, *PLoS One*, 2008, **3**, e2351.
164 J. Yu, J. Xiao, X. Ren, K. Lao and X. S. Xie, *Science*, 2006, **311**, 1600–1603.
165 A. Leutenegger, C. D'Angelo, M. V. Matz, A. Denzel, F. Oswald, A. Salih, G. U. Nienhaus and J. Wiedenmann, *FEBS J.*, 2007, **274**, 2496–2505.
166 A. Terskikh, A. Fradkov, G. Ermakova, A. Zaraisky, P. Tan, A. V. Kajava, X. Zhao, S. Lukyanov, M. Matz, S. Kim, I. Weissman and P. Siebert, *Science*, 2000, **290**, 1585–1588.
167 H. W. Ai, K. L. Hazelwood, M. W. Davidson and R. E. Campbell, *Nat. Methods*, 2008, **5**, 401–403.
168 S. Karasawa, T. Araki, T. Nagai, H. Mizuno and A. Miyawaki, *Biochem. J.*, 2004, **381**, 307–312.
169 G. J. Kremers, J. Goedhart, E. B. van Munster and T. W. Gadella Jr, *Biochemistry*, 2006, **45**, 6570–6580.
170 A. J. Lam, F. St-Pierre, Y. Gong, J. D. Marshall, P. J. Cranfill, M. A. Baird, M. R. McKeown, J. Wiedenmann, M. W. Davidson, M. J. Schnitzer, R. Y. Tsien and M. Z. Lin, *Nat. Methods*, 2012, **9**, 1005–1012.
171 Y. Wang, J. Y. Shyy and S. Chien, *Annu. Rev. Biomed. Eng.*, 2008, **10**, 1–38.
172 K. B. Bravaya, O. M. Subach, N. Korovina, V. V. Verkhusha and A. I. Krylov, *J. Am. Chem. Soc.*, 2012, **134**, 2807–2814.
173 P. Bell, L. H. Vandenberghe, D. Wu, J. Johnston, M. Limberis and J. M. Wilson, *J. Histochem. Cytochem.*, 2007, **55**, 931–939.
174 O. V. Stepanenko, D. M. Shcherbakova, I. M. Kuznetsova, K. K. Turoverov and V. V. Verkhusha, *BioTechniques*, 2011, **51**, 313–327.
175 M. Z. Lin, M. R. McKeown, H. L. Ng, T. A. Aguilera, N. C. Shaner, R. E. Campbell, S. R. Adams, L. A. Gross, W. Ma, T. Alber and R. Y. Tsien, *Chem. Biol.*, 2009, **16**, 1169–1179.
176 A. G. Evdokimov, M. E. Pokross, N. S. Egorov, A. G. Zaraisky, I. V. Yampolsky, E. M. Merzlyak, A. N. Shkoporov, I. Sander, K. A. Lukyanov and D. M. Chudakov, *EMBO Rep.*, 2006, **7**, 1006–1012.
177 H. Katayama, A. Yamamoto, N. Mizushima, T. Yoshimori and A. Miyawaki, *Cell Struct. Funct.*, 2008, **33**, 1–12.
178 D. Shcherbo, C. S. Murphy, G. V. Ermakova, E. A. Solovieva, T. V. Chepurnykh, A. S. Shcheglov, V. V. Verkhusha, V. Z. Pletnev, K. L. Hazelwood, P. M. Roche, S. Lukyanov,

 

A. G. Zaraisky, M. W. Davidson and D. M. Chudakov, *Biochem. J.*, 2009, **418**, 567–574.
179 S. J. Remington, *Curr. Opin. Struct. Biol.*, 2006, **16**, 714–721.
180 S. Pletnev, N. G. Gurskaya, N. V. Pletneva, K. A. Lukyanov, D. M. Chudakov, V. I. Martynov, V. O. Popov, M. V. Kovalchuk, A. Wlodawer, Z. Dauter and V. Pletnev, *J. Biol. Chem.*, 2009, **284**, 32028–32039.
181 M. E. Bulina, K. A. Lukyanov, O. V. Britanova, D. Onichtchouk, S. Lukyanov and D. M. Chudakov, *Nat. Protocols*, 2006, **1**, 947–953.
182 C. Coltharp and J. Xiao, *Cell. Microbiol.*, 2012, **14**, 1808–1818.
183 B. O. Leung and K. C. Chou, *Appl. Spectrosc.*, 2011, **65**, 967–980.
184 T. Müller, C. Schumann and A. Kraegeloh, *ChemPhysChem*, 2012, **13**, 1986–2000.
185 G. Ball, R. M. Parton, R. S. Hamilton and I. Davis, *Methods Enzymol.*, 2012, **504**, 29–55.
186 R. Henriques, C. Griffiths, E. Hesper Rego and M. M. Mhlanga, *Biopolymers*, 2011, **95**, 322–331.
187 J. Lippincott-Schwartz and G. H. Patterson, *Trends Cell Biol.*, 2009, **19**, 555–565.
188 T. Dertinger, R. Colyer, R. Vogel, J. Enderlein and S. Weiss, *Opt. Express*, 2010, **18**, 18875–18885.
189 M. Bossi, J. Fölling, M. Dyba, V. Westphal and S. W. Hell, *New J. Phys.*, 2006, **8**, 275.
190 C. E. Shannon, *Proc. IRE*, 1949, **37**, 10–21.
191 B. Hein, K. I. Willig and S. W. Hell, *Proc. Natl. Acad. Sci. U. S. A.*, 2008, **105**, 14271–14276.
192 U. V. Nägerl, K. I. Willig, B. Hein, S. W. Hell and T. Bonhoeffer, *Proc. Natl. Acad. Sci. U. S. A.*, 2008, **105**, 18982–18987.
193 J. Tonnesen, F. Nadrigny, K. I. Willig, R. Wedlich-Soldner and U. V. Nägerl, *Biophys. J.*, 2011, **101**, 2545–2552.
194 P. N. Hedde, J. Fuchs, F. Oswald, J. Wiedenmann and G. U. Nienhaus, *Nat. Methods*, 2009, **6**, 689–690.
195 Y. Li, Y. Ishitsuka, P. N. Hedde and G. U. Nienhaus, *ACS Nano*, 2013, **7**, 5207–5214.
196 T. Quan, P. Li, F. Long, S. Zeng, Q. Luo, P. N. Hedde, G. U. Nienhaus and Z.-L. Huang, *Opt. Express*, 2010, **18**, 11867–11876.
197 C. S. Smith, N. Joseph, B. Rieger and K. A. Lidke, *Nat. Methods*, 2010, **7**, 373–375.
198 S. W. Hell, *Nat. Methods*, 2009, **6**, 24–32.
199 M. G. Gustafsson, *J. Microsc.*, 2000, **198**, 82–87.
200 E. H. Rego, L. Shao, J. J. Macklin, L. Winoto, G. A. Johansson, N. Kamps-Hughes, M. W. Davidson and M. G. Gustafsson, *Proc. Natl. Acad. Sci. U. S. A.*, 2012, **109**, E135–E143.
201 R. E. Thompson, D. R. Larson and W. W. Webb, *Biophys. J.*, 2002, **82**, 2775–2783.
202 K. Finan, B. Flottmann and M. Heilemann, *Methods Mol. Cell. Biol.*, 2013, **950**, 131–151.
203 P. Annibale, M. Scarselli, A. Kodiyan and A. Radenovic, *J. Phys. Chem. Lett.*, 2010, **1**, 1506–1510.
204 H. Mizuno, P. Dedecker, R. Ando, T. Fukano, J. Hofkens and A. Miyawaki, *Photochem. Photobiol. Sci.*, 2010, **9**, 239–248.
205 L. Kastrup, H. Blom, C. Eggeling and S. W. Hell, *Phys. Rev. Lett.*, 2005, **94**, 178104.
206 P. N. Hedde, R. M. Dörlich, R. Blomley, D. Gradl, E. Oppong, A. C. B. Cato and G. U. Nienhaus, *Nat. Commun.*, 2013, **4**, 2093.
207 W. Tomosugi, T. Matsuda, T. Tani, T. Nemoto, I. Kotera, K. Saito, K. Horikawa and T. Nagai, *Nat. Methods*, 2009, **6**, 351–353.
208 M. A. Mena, T. P. Treynor, S. L. Mayo and P. S. Daugherty, *Nat. Biotechnol.*, 2006, **24**, 1569–1571.
209 H. W. Ai, N. C. Shaner, Z. Cheng, R. Y. Tsien and R. E. Campbell, *Biochemistry*, 2007, **46**, 5904–5910.
210 O. M. Subach, I. S. Gundorov, M. Yoshimura, F. V. Subach, J. Zhang, D. Gruenwald, E. A. Souslova, D. M. Chudakov and V. V. Verkhusha, *Chem. Biol.*, 2008, **15**, 1116–1124.
211 J. Goedhart, L. van Weeren, M. A. Hink, N. O. Vischer, K. Jalink and T. W. Gadella Jr, *Nat. Methods*, 2010, **7**, 137–139.
212 M. A. Rizzo, G. H. Springer, B. Granada and D. W. Piston, *Nat. Biotechnol.*, 2004, **22**, 445–449.
213 A. B. Cubitt, R. Heim, S. R. Adams, A. E. Boyd, L. A. Gross and R. Y. Tsien, *Trends Biochem. Sci.*, 1995, **20**, 448–455.
214 H. W. Ai, J. N. Henderson, S. J. Remington and R. E. Campbell, *Biochem. J.*, 2006, **400**, 531–540.
215 H. Tsutsui, S. Karasawa, Y. Okamura and A. Miyawaki, *Nat. Methods*, 2008, **5**, 683–685.
216 S. Karasawa, T. Araki, M. Yamamoto-Hino and A. Miyawaki, *J. Biol. Chem.*, 2003, **278**, 34167–34171.
217 A. B. Cubitt, L. A. Woollenweber and R. Heim, *Methods Cell Biol.*, 1999, **58**, 19–30.
218 H. W. Ai, S. G. Olenych, P. Wong, M. W. Davidson and R. E. Campbell, *BMC Biol.*, 2008, **6**, 13.
219 O. Zapata-Hommer and O. Griesbeck, *BMC Biotechnol.*, 2003, **3**, 5.
220 N. C. Shaner, G. G. Lambert, A. Chammas, Y. Ni, P. J. Cranfill, M. A. Baird, B. R. Sell, J. R. Allen, R. N. Day, M. Israelsson, M. W. Davidson and J. Wang, *Nat. Methods*, 2013, **10**, 407–409.
221 A. Miyawaki, O. Griesbeck, R. Heim and R. Y. Tsien, *Proc. Natl. Acad. Sci. U. S. A.*, 1999, **96**, 2135–2140.
222 T. Nagai, K. Ibata, E. S. Park, M. Kubota, K. Mikoshiba and A. Miyawaki, *Nat. Biotechnol.*, 2002, **20**, 87–90.
223 O. Griesbeck, G. S. Baird, R. E. Campbell, D. A. Zacharias and R. Y. Tsien, *J. Biol. Chem.*, 2001, **276**, 29188–29194.
224 N. C. Shaner, M. Z. Lin, M. R. McKeown, P. A. Steinbach, K. L. Hazelwood, M. W. Davidson and R. Y. Tsien, *Nat. Methods*, 2008, **5**, 545–551.
225 A. Sakaue-Sawano, H. Kurokawa, T. Morimura, A. Hanyu, H. Hama, H. Osawa, S. Kashiwagi, K. Fukami, T. Miyata, H. Miyoshi, T. Imamura, M. Ogawa, H. Masai and A. Miyawaki, *Cell*, 2008, **132**, 487–498.

226 T. Kogure, S. Karasawa, T. Araki, K. Saito, M. Kinjo and A. Miyawaki, *Nat. Biotechnol.*, 2006, **24**, 577–581.
227 L. Wang, W. C. Jackson, P. A. Steinbach and R. Y. Tsien, *Proc. Natl. Acad. Sci. U. S. A.*, 2004, **101**, 16745–16749.
228 K. S. Morozova, K. D. Piatkevich, T. J. Gould, J. Zhang, J. Bewersdorf and V. V. Verkhusha, *Biophys. J.*, 2010, **99**, L13–L15.
229 K. D. Piatkevich, V. N. Malashkevich, K. S. Morozova, N. A. Nemkovich, S. C. Almo and V. V. Verkhusha, *Surf. Sci. Rep.*, 2013, **3**, 1847.
230 F. V. Subach, O. M. Subach, I. S. Gundorov, K. S. Morozova, K. D. Piatkevich, A. M. Cuervo and V. V. Verkhusha, *Nat. Chem. Biol.*, 2009, **5**, 118–126.
231 T. Tsuboi, T. Kitaguchi, S. Karasawa, M. Fukuda and A. Miyawaki, *Mol. Biol. Cell*, 2010, **21**, 87–94.
232 R. Ando, C. Flors, H. Mizuno, J. Hofkens and A. Miyawaki, *Biophys. J.*, 2007, **92**, L97–L99.
233 O. M. Subach, V. N. Malashkevich, W. D. Zencheck, K. S. Morozova, K. D. Piatkevich, S. C. Almo and V. V. Verkhusha, *Chem. Biol.*, 2010, **17**, 333–341.



 